FINAL REPORT
MARCH 1969

CRACK INITIATION AT NOTCHES IN LOW CYCLE FATIGUE

BY

V. Weiss, M. Ogasawara,
M. Adachi and J. Sessler

SPONSORED BY
OFFICE OF RESEARCH GRANTS AND CONTRACTS
NATIONAL AERONAUTICS AND SPACE ADMINISTRATION
WASHINGTON, D.C.

CONTRACT NO. NGR-33-022-023
CONTRACT PERIOD: 1 August 1968 - 15 March 1969

SYRACUSE UNIVERSITY RESEARCH INSTITUTE
DEPARTMENT OF CHEMICAL ENGINEERING AND METALLURGY
MET.E. 1313-15369-F

ACKNOWLEDGMENTS

The authors wish to express their special thanks to the useful advice given by Dr. H. W. Liu, Professor of Syracuse University and the significant contributions made by the previous investigator connected with the project, W. MacInnes. Thanks are also due to Mr. C. Chave and Mr. K. Chapman for their assistance in the technical program. Mrs. H. Turner and Mrs. B. Howden aided in the preparation of the manuscript.

The authors are also indebted to the National Aeronautics and Space Administration for sponsoring this research.

ABSTRACT

An experimental study of the plastic strain distribution near notches was undertaken to aid in the analysis of low cycle fatigue crack initiation. It was found that the strain at the notch root can be readily obtained from measurement of the root radius change and is given by $\varepsilon_{NR} = \ln \sqrt{\frac{\rho}{\rho_o}}$. Away from the notch root, the longitudinal strain decreases as $(1/\text{distance})^m$, with $m = 0.5 \sim 0.67$, i.e., not too different from the strain distribution predicted from the theory of elasticity. This similarity between elastic and plastic strain distribution for AM 350 steel sheet is further confirmed by the experimental result that the true strain concentration factor is approximately equal to the elastic stress concentration factor, and is certainly related to the strain hardening behavior of the test material.

Analyses of the present data on crack initiation in 7075-T6 aluminum show that a Manson-Coffin type relationship obtains, provided that plastic constraint is taken into account, $N_o^{\frac{1}{2}} \varepsilon_{p,NR}^{tr} = \text{const}$. If the total strain range at the notch root is considered, the exponent on N_0 in the Manson-Coffin reslationship is 1/4 rather than 1/2. The energy loss per cycle, as determined from the hysterisis loops, may also serve as a useful parameter in the analysis of crack initiation. For the present data one obtains that the product of energy loss per cycle and number of cycles to crack initiation is constant.

CONTENTS

LIST OF FIGURES

LIST OF TABLES

TABLE

I. INTRODUCTION

Reasonable interpretations of the crack propagation behavior in strain controlled low cycle fatigue have been given,[1-5,18] generally in the form,

$$\frac{dc}{dN} \simeq c^{\beta} \left(\frac{\varepsilon^{tr}}{\varepsilon_o}\right)^{\beta'} \qquad (1)$$

Where, c is the crack length, ε^{tr} the total strain range, β, β' and ε_o are constants. Manson and coworkers[1,2]* suggested $\beta \simeq 1$ if the plastic component of ε^{tr}, ε_p^{tr}, is used. The value of β' is related to the fatigue strain hardening exponent and could range between 1 and 2. Weiss and co-workers[11,12] have found β' between 1.69 and 2 for 7075-T6 aluminum. Boettner, Laird and McEvily[6] find $\beta \simeq 1$ and $\beta' \simeq 2$ for OFHC copper, and suggested the use of a strain intensity factor, $\varepsilon^{tr}\sqrt{c}$, analogous to the stress intensity factor ΔK.

According to all these analyses, a crack under constant stress or strain amplitude will accelerate to final failure. In a macroscopic sense, crack propagation is a "regular" behavior, mostly because of the repetition of almost identical conditions during each cycle; plastic zone growth → rounding of tip radius → crack propagation → closing and sharpening of crack in compression.

Once a crack has grown to a sufficient length, the stress and strain fields ahead of the crack show little influence of the original geometric stress concentration that caused the crack initiation.

*Numbers in parenthesis refer to references at the end of the text.

An analysis of crack initiation in strain controlled fatigue, however, is more complicated for several primary reasons:

1) Lack of adequate plasticity solutions for the type of stress concentration responsible for crack initiation.
2) The need to define the crack initiation in terms of an observable crack length.
3) Difficulties in uniquely defining net section strain in a notched specimen.

Manson and Hirschberg[1] have obtained an empirical relationship of fatigue crack initiation for smooth specimens from the macroscopic point of view as:

$$N_o = N_f - 4N_f^{0.6} \tag{2}$$

where, N_o is defined as the number of cycles to initiate a crack of engineering size, and N_f, is the number of cycles to failure. It is obtained from the well known Manson-Coffin[15] equation.

$$N_f (\varepsilon^{tr})^2 = \text{const} \tag{3}$$

Here ε^{tr} is the strain range. For notched specimens, Manson[2] assumed that crack initiation depends only on the localized strain range at the root of the notch. Thus, Equation (2), obtained for smooth specimens, could be applied to notched specimens and the local strain range at the notch root, ε_{NR}^{tr}, is obtained from

$$\varepsilon_{NR}^{tr} = \varepsilon^{tr} K_\varepsilon \tag{4}$$

where K_ε is the strain concentration factor. Generally accepted analytical solutions for the strain concentration factor, K_ε, are still lacking though

Hardrath& Ohman[16] and Neuber[17] have proposed relationships between the elastic stress concentration factor and the true stress or strain concentration factors. For the notch geometry and material (Al-7075 and 4340 steel) studied by Manson[2], both relationships[16,17] yield nearly the same value for K_ε and the experimental results are in fair agreement with the predictions of Equation (2). The presence of a crack of length 0.006 to 0.010 was used to define N_0.

The validity of Neuber's rule[17] for fatigue life prediction of Al 2024-T6 was also investigated by R. M. Wetzel[7]. Both Manson and Wetzel conclude that the strain concentration factor, K_ε, calculated from Neuber's rule, predicts the maximum strain at the notch root quite accurately and that the maximum strain range is indeed the controlling factor for fatigue crack initiation.

Recently, C. Laird and A. R. Krause[8] have studied the relationship betwen N_o and the plastic component of the total strain range, for smooth specimens, ε_p^{tr}, and find

$$N_o \, (\varepsilon_p^{tr})^\alpha = \text{const} \qquad (5)$$

Their calculations predict $\alpha \simeq 1$ to 1.5 and the experimental results yield $\alpha = 1$ (plasticine) to $\alpha = 2$ (nickel). The calculations were based on the assumption that the specimen cross section will undergo shape changes during strain cycling. Such a process is self accelerating and thin sections become thinner as the material "lost" is redistributed into the thicker sections. Gradually one of the thin sections becomes the dominant crack. If the

total strain range, ε^{tr}, is used in the analysis of Manson's data[2] the exponent α of Equation (5) is estimated to lie between 3 and 5.

Low cycle stress controlled fatigue tests ($200<N_f<10^5$) on notched sheet specimens of Al 2024-T3 by Crew[9] indicate that the data can be well reconciled with an analysis based on the assumption that the local maximum stress is the controlling factor. Stresses were measured by strain gages located at the root of the notch ($K_t = 2$) and were found to be in agreement with the Hardrath and Ohman prediction[16]. It should be noted that a unique relationship exists between stress and strain after shakedown, i.e. a constant stress range also corresponds to a constant plastic strain range and it would consequently be impossible to decide from continuum mechanics whether the stress or the strain range is responsible for crack initiation. For the very low cycle range, strain is preferred as the controlling variable because of the general shape of the stress strain curve for large strains, where an error in stress control can result in considerably larger variations in life than an error in strain control. The microscopic argument concerning the mechanism of crack initiation has not been resolved.

Recently Weiss et al.[3,5,11,12] have reported on crack initiation in low cycle strain controlled fatigue of notched Al 7075-T6 specimens. The strain concentration factor K_ε, in itself a function of the strain range, was obtained with the help of Neuber's rule and is given by

$$K_\varepsilon\ (\varepsilon^{tr}) \equiv K_t\ \gamma(\varepsilon^{tr}) \tag{6}$$

with $\gamma(\varepsilon^{tr})$ ranging from 1 to 2. To obtain the effective plastic strain

near the notch root, $\varepsilon^{tr}_{p,NR}$ plastic constraint was taken into account

$$\varepsilon^{tr}_{p,NR} = K_\varepsilon \varepsilon^{tr} - 1.5\ (2\varepsilon_Y) \tag{7}$$

where ε_Y is the yield strain, σ_Y/E, and 1.5 is the constraint factor. A Manson-Coffin type relationship between N_o and $\varepsilon^{tr}_{p,NR}$ is obtained for the crack initiation data:

$$N_o^{0.5}\ (K_\varepsilon \varepsilon^{tr} - 3\varepsilon_Y) = \text{const} \tag{8}$$

Hence they propose that crack initiation in notched specimens can be interpreted as the failure of a small ligament near the notch root subjected to the same strain cycling history.

The present work is an extension of these efforts. Careful measurements and analyses of the strain distributions near notch roots made it possible to devise a simple method for directly measuring the strain range at the notch root. Experimental studies on three notch geometries (notch depth 30%, K_t=2,3,4) are presented and analyzed in light of this more detailed understanding of the stress and strain distributions in the plastic range near the notch root.

II. EXPERIMENTAL

A. Local Strain Distribution Near the Notch Root

The plastic strain distribution has been studied for a variety of notch geometries in annealed AM-350 steel sheet (σ_{TU}=190 ksi, σ_Y=70 ksi; thickness = 0.062 in). The specimen design is shown in Figure 1. Theoretical elastic stress concentration factors[14] ranged from 2 to 12.5. The strain distribution was obtained from measurements on a 200 lines per inch grid printed on the flat surface of the specimen by photoresist methods. All measurements were made on the specimens after unloading. Figure 2 shows the measured longitudinal plastic strain distribution along the line connecting the notch roots. This plastic strain is correlated to the theoretical elastic strain calculated by Neuber[13] from the elastic theory in Figure 3.

The maximum strain at the notch root is of special interest. It was obtained from an extrapolation procedure based on an approximate strain distribution near notch roots suggested by Weiss[4], namely

$$\frac{\varepsilon_y}{\varepsilon_n} = \left(K_t\sqrt{\frac{\rho}{\rho+4x}}\right)^{2/(n+1)} \qquad (9)$$

where $0 \leq n \leq 1$. Hence a plot of ln ε_y vs. ln $(x+\frac{\rho}{4})$ should yield straight lines. The maximum strain at the notch root is obtained from an extrapolation of these straight lines to x = 0. The results, shown in Figure 4, clearly justify the use of this method as the data points lie on straight lines and the extrapolation distance is small compared to the span over which data points lie on straight lines. It should be noted that the

slope of these lines, $\frac{1}{n+1}$, is between 0.5 and 0.67, corresponding to an effective strain hardening exponent $0.5 \leq n \leq 1$. These results as well as those presented in Figure 3 indicate that for AM-350 steel the plastic strain distribution is not too different from the elastic strain distribution[13].

Geometrical considerations of the deformation of a parabolic or hyperbolic notch suggest an additional method for the determination of the maximum strain at the notch root. If the general parabolic or hyperbolic shape is retained, the true maximum strain at the root is given by

$$\varepsilon_{NR} = \ln \sqrt{\frac{\rho}{\rho_o}} \tag{10}$$

where ρ is the instantaeous root radius and ρ_o the root radius before loading. Figure 5 shows the root radius change as a function of the notch root strain obtained by the extrapolation method (Figure 4). The solid curve, representing the relationship of Equation 10, is seen to be in good agreement with the data, except for strains above 35%, where plastic constraint and residual stress effects may have affected the results. These results then give confidence to the use of this simple method for determining the notch root strain from measurements of the notch root radius. Thus the total strain range at the base of a notch can be obtained from

$$\varepsilon_{NR}^{tr} = \ln \sqrt{\frac{\rho_T}{\rho_C}} \tag{11}$$

where ρ_T is the root radius at maximum nominal strain (tension) and ρ_C the root radius at minimum nominal strain (compression).

The strain concentration factor, K_ε, can now also be determined. It is defined as the ratio of maximum strain to average net section strain.

Experimental difficulties exist in the determination of the average net section strain, ε_n, which can be obtained a) by forming the average across the minimum section e.g. from distributions such as illustrated in Figure 2 and adding the yield strain and b) from the uniaxial true stress-strain curve as that total strain which corresponds to the nominal net section stress. For the present results on AM-350 steel the former method (a) yields slightly lower values for ε_n. The results for both methods are presented in Figure 6 where the strain concentration factors are plotted as a function of the theoretical elastic stress concentration factors[14]. It appears that $K_\varepsilon \simeq K_t$ represents a good approximation which is again in agreement with the results presented in Figures 3 and 4. Table I is a summary of the results obtained on the AM-350 steel sheet specimens.

B. Fatigue Crack Initiation Studies

The previous preliminary study on fatigue crack initiation on Al 7075-T6 was conducted with very shallow circumferential notches in order to minimize the ambiguity concerning the net section strain[5]. The results on the strain distribution in the plastic range, discussed in the previous section A, make it now possible to study crack initiation from deeper notches and to independently ascertain the strain cycling range at the notch root and the nominal net section strain. However, to facilitate the optical measurement of the root radius changes, specimens having a rectangular crossection were used, Figure 7. The chemical composition and the standard mechanical properties of Al 7075-T6 used in this and the previous[5] study are given in Table II.

The notch depth was 30%, the notch angle 60° and the elastic stress concentration factors were 2, 3, and 4 with corresponding root radii of 0.06 in, 0.02 in and 0.01 in. The notch root was slightly polished using 3/0 metallographic polishing paper.

The fatigue tests were conducted in the same set-up as used previously by Rabaut[11] and MacInnes[12]. The total strain range is controlled, as before, from the strain gauge extensometer spanning a gauge length of 0.300 in. The extensometer is calibrated on a micrometer to within $\pm 5 \times 10^{-5}$ inches and the error in the determination of the strain on the chart is $\pm$ 0.01%.

The compliance method was essentially used to determine the number of cycles to crack initiation, N_o. Since 7075-T6 aluminum produces very stable hysteresis loops and neither fatigue hardens nor fatigue softens noticeably, the occurence of a 3-4% drop in peak load was used to define N_o, Figure 8. This method yielded reliable and reproducible results and corresponds to crack lengths of 0.001 to 0.010 in. in depth. Typical cracks appearing at the notch root, for fatigue lives somewhat above N_o, are shown in Figure 9. A cross sectional view of an area near the principal crack is shown in Figure 10, which indicates that stage I crack initiation occurs over a large area of the notch root.

The strain range at the notch root was calculated according to Equation 11. The corresponding root radii were obtained from photographs taken periodically during the test at the maximum (ρ_T) and the minimum (ρ_C) net section strain. The approximate error of the optical measurements is $\pm$ 2%, which results in a relative error of $\pm$ 1% in the strain range at the notch root.

The experimental results relating the total strain range at the notch root and number of cycles to crack initiation are shown in Figure 11. The present data seem to follow a relationship

$$N_o^{\frac{1}{4}} \varepsilon_{NR}^{tr} = \text{const} \qquad (12)$$

and lie between the relationship proposed by Manson, Equation 2, and the failure curve obtained in previous studies[2,12].

To obtain the plastic component of the total strain range at the notch root, it is necessary to determine and subtract the elastic contribution, σ_Y/E, where σ_Y is the yield strength and E is Young's modulus[5]. The value of the effective yield strength in the vicinity of the notch will be higher than the uniaxial yield strength due to plastic constraint. For the present geometry the maximum constraint factor, μ, in the plane strain region ahead of the crack is 2.3[5] i.e. yielding would initiate at a local stress equal to 2.3 times the uniaxial yield strength. The local constraint factor is a function of position, η, below the notch root and the root radius ρ, Figure 12. Since the phenomena responsible for crack initiation are believed to occur in a small volume just below the notch root, it seems reasonable to select $\eta = 5 \times 10^{-3}$ in, i.e. approximately the same depth as the crack depth used to define N_o. Thus the plastic strain range at the notch root is given by

$$\varepsilon_{p,NR}^{tr} = \varepsilon_{NR}^{tr} - \mu \varepsilon_Y^{cycle} \qquad (13)$$

where the elastic yield strain range, ε_Y^{cycle} is obtained from the cyclic

stress strain curve. For the three notch geometry investigated the constraint factors are μ = 1.25, 1.41, and 1.62, corresponding to root radii of 0.06, 0.02, and 0.01. In Figure 13 is shown the effective plastic strain at the notch root, Equation 13, versus the number of cycles to crack initiation. The data clearly follow a Manson-Coffin type relationship, namely

$$N_o^{\frac{1}{2}} \varepsilon_{p,NR}^{tr} = \text{const} \qquad (14)$$

in agreement with previous observations[5]. However, the notch root strain range was obtained directly in the present study, while it was inferred from Neuber's rule[17], i.e. the calculation of strain concentration factors, in the former study[5].

An analysis of the hysteresis loops obtained from the present tests can also yield information about the strain range in the plastic zone. The energy absorption per cycle, i.e. the area inside the hysteresis loop, is the direct result of plastic deformation near the notch roots. Assuming an ideally plastic material, yield strength equal to σ_Y, the plastic work is given by

$$W_p = \int_{\varepsilon = \varepsilon_Y}^{\varepsilon_{p,NR}^{tr}} \int \sigma_Y \, d\varepsilon dV \qquad (15)$$

where: $dV = 2\pi\zeta t x dx$; ζ is a shape factor, t the specimen thickness and x the distance from the notch root. For the ideally plastic case[4]

$$\frac{\varepsilon}{\varepsilon_{NR}} = \frac{\rho}{\rho + 4x} \qquad (16)$$

which yields

$$x = \frac{\rho}{4}\left\{ \left(\frac{\varepsilon_{NR}}{\varepsilon}\right) - 1 \right\} \tag{17}$$

where ε is the local strain and ε_{NR} the maximum strain at the notch root. Combining Equations 15 and 17 yields for the plastic work per cycle

$$W_p = \zeta \frac{\pi t \rho^2 \sigma_Y}{16} \int_{\varepsilon = \varepsilon_Y}^{\varepsilon^{tr}_{p,NR}} \left(\frac{\varepsilon_{p,NR}}{\varepsilon} - 1\right)^2 d\varepsilon \tag{18}$$

or for $\varepsilon_{p,NR} >> \varepsilon_Y$

$$W_p = \zeta \frac{\pi t \rho^2 \sigma_Y}{16} \cdot \varepsilon_Y \cdot \left(\frac{\varepsilon^{tr}_{p,NR}}{\varepsilon_Y}\right)^2 \tag{19}$$

with $\varepsilon^{tr}_{p,NR}$ being the strain range at the notch root and ε_Y the strain corresponding to the yield stress corrected for triaxiality. For a plastic strain distribution of the character observed in the AM 350 specimens discussed previously, i.e.

$$\frac{\varepsilon}{\varepsilon_{NR}} = \left(\frac{\rho}{\rho + 4x}\right)^{\frac{1}{2}} \tag{20}$$

one obtains for the plastic work per cycle ($\varepsilon^{tr}_{p,NR} >> \varepsilon_Y$),

$$W_p = \zeta \frac{\pi t \rho^2 \sigma_Y}{48} \cdot \varepsilon_Y \cdot \left(\frac{\varepsilon^{tr}_{p,NR}}{\varepsilon_Y}\right)^4 \tag{21}$$

Figure 14 shows a plot of $\ln \frac{W_p}{\sigma_Y t \rho^2}$ vs. $\ln \varepsilon^{tr}_{p,NR}$. The latter was corrected for plastic constraint in accordance with Equation 13. The energy absorption values were obtained from the hysteresis loops and the strain ranges at the notch root were obtained from root radius measurements, Equation 11. The data shown in Figure 14 are in good agreement with Equation 19, which resulted from the assumption of an ideally plastic strain distribution, $\varepsilon \sim 1/x$. Figure 15 shows the relationship between plastic energy absorption per cycle and the number of cycles to crack initiation. The data fall in a scatterband around

$$\frac{W_p}{\sigma_Y t \rho^2} \cdot N_o = \text{const} \qquad (22)$$

as predictable from Figures 13 and 14. The experimental data are summarized in Table III.

III. DISCUSSION AND CONCLUSIONS

The experimental results on the plastic strain distribution near notches in annealed AM350 sheet specimens discussed in IIA indicate that the plastic strains have nearly the same dependence on distance from the notch root as do the theoretical elastic strains, Equation 9, $0.5 < n < 1$. This is no doubt due to the high degree of strain hardening of the material, which had a uniform elongation of $\varepsilon_u \approx 0.25$. Similar results have been obtained by H. W. Liu et al.[17] on 7075-T6 and 2024-T351 aluminum alloys, $n \approx 1$, and on Al 2024-0, $n \approx 0.4$. From the stress strain curve and the elastic stress concentration factor, it is also possible[16] to obtain values for the true stress and the true strain concentration factors. These are indicated in Figure 6 and are in fair agreement with the experimentally determined values.

Measurement of the root radius change for the determination of notch root strain, Equation 10, has proven a valuable tool for the analysis of fracture and low cycle fatigue of notched specimens. With suitable experimental arrangements (photographic etc.) it should be possible to measure the root radius changes at mid-thickness, where a condition of plane strain might exist for small root radii, although this was not attempted in the present study.

The energy loss per fatigue cycle provides another means of analyzing fatigue data. Although the realtionships used for the present analysis are approximated, Equations 15 - 19, the potential of the method is clearly evident. Further refinements in plastic strain analyses near notches and

cracks are desirable, especially for the transition from plane strain to the strain distribution on the faces, which affects the calculation of the test volume contributing to the energy loss.

From the experimental data and this analysis it may be concluded that the energy loss per cycle should be considered as a useful parameter for the analysis of crack initiation in low cycle fatigue, Figure 15 and Equation 22. Direct strain measurements at the notch root yield a Manson-Coffin type relationship for crack initiation, provided that plastic constraint is taken into account, Equation 14. If the total strain range at the notch root is considered, the exponent on N_o in the Manson-Coffin relationship is 1/4 rather than 1/2.

SYMBOLS

A: B: C: Specimen series notations of 7075-T6 Aluminum

A: $K_t = 2$ ($\rho = 0.06$ in.)

B: $K_t = 3$ ($\rho = 0.02$ in.)

C: $K_t = 4$ ($\rho = 0.01$ in.)

D: Specimen total width

E: Young's modulus

K: Stress intensity factor

K_t: Geometrical stress concentration factor

K_ε: Strain concentration factor

K_ε^{ave}: Strain concentration factor defined by $\dfrac{\varepsilon_{p,NR}}{\varepsilon_p^{ave}+\varepsilon_Y}$

K_ε^n: Strain concentration factor defined by $\dfrac{\varepsilon_{p,NR}}{\varepsilon_n}$

N: Number of cycles

N_o: Number of cycles to initiate a crack of engineering size

N_f: Number of cycles to failure

P: Applied load

ΔP^{tr}: Total cyclic load

(Difference between the maximum tension load and the maximum compression load)

S: The minimum cross section of the notched specimen.

TU: Specimen series notation of AM-350 stainless steel

(Specimens are taken in transverse to the rolling direction)

V: Volume of the plastically deformed zone

W_p: The plastic energy absorbed per cycle

---

c: Half crack length or notch depth

d: Specimen width at the minimum cross section

l: Gauge length

Δl_p: Plastic extension due to hysteresis loop

n: Exponent

t: Specimen thickness

x: Distance from the notch root
(Direction normal to the applied load)

y: Distance from the minimum cross section
(Direction parallel to the applied load)

α: The constant exponent in the Manson type relations

β, β': The constant exponents

γ: Constant

ε_o: Constant

ε_Y: Yield strain

ε_n: Nominal strain obtained from the uniaxial stress-strain curve
(Corresponding to the nominal stress $\sigma_n = P/S$)

ε_p^{ave}: Plastic strain averaged across the minimum cross section

ε_e^+: Elastic constraint strain

ε_Y^{cycle}: Cyclic yield strain

ε_{NR}: The maximum strain at the notch root (Notch root strain)

$\varepsilon_{p,NR}$: The maximum plastic strain at the notch root

ε^{tr}: Total strain range under fatigue load defined by

$$\varepsilon^{tr} = \varepsilon^{tension} - \varepsilon^{compression}$$

ε_p^{tr}: Total plastic strain range

ε_{NR}^{tr}: Total strain range at the notch root

$\varepsilon_{p,NR}^{tr}$: Plastic total effective strain range at the notch root defined by $\varepsilon_{p,NR}^{tr} = \varepsilon_{NR}^{tr} - \varepsilon_e^+$

$\varepsilon_y(y=0)$: Strain in y-direction on y=0 plane

$\varepsilon_{y,p}$: Plastic strain in y-direction on y=0 plane

ε_e^{theory}: Elastic strain calculated by Neuber

ε_p^{exp}: Plastic strain measured by grid method

θ: Angle change between the boundaries along the shear stress trajectories

η: Crack depth for which N_o is defined

μ: Elastic constraint factor

ρ: Root radius

ρ_o: Original root radius

ρ_T: Root radius at the maximum tension load

ρ_c: Root radius at the maximum compression load

$\Delta\rho$: Root radius change defined by $\Delta\rho = \rho - \rho_o$

σ: Stress

σ_n: Nominal engineering stress obtained by $\sigma_n = P/S$

σ_y: Stress parallel to the direction of load

σ_x: Stress normal to the direction of load

σ_{TU}: Tensile ultimate high strength

σ_Y: Yield strength

ζ: Geometrical correction factor for plastic zone

REFERENCES

1. S. S. Manson, "Interface Between Fatigue, Creep, and Fracture," NASA Technical Memorandum NASA TM X-52189. Proc. of the First Int. Conf. on Fracture, Sendai, Japan, Vol.3, pp. 1387-1432 (1966).

2. S. S. Manson and M. H. Hirschberg, "Crack Initiation and Propagaton in Notched Fatigue Specimens," NASA TM X-52126. Proc. of the First Int. Conf. on Fracture, Sendai, Japan, Vol. 1, pp. 479-498 (1966.).

3. V. Weiss, "Fatigue," Proc. of the Tenth Sagamore Army Materials Research Conf., Syracuse University Press, (1964).

4. V. Weiss, "Notch Analysis of Fracture," in book Treatise on Fracture, ed. H. Liebowitz Academic Press, to be published.

5. V. Weiss, G. Rabaut, and W. MacInnes, "Crack Propagation and Initiation in Low Cycle Strain Controlled Fatigue," Czech. J. Phys. B 19 (1969).

6. R. C. Boettner, C. Laird, and A. J. McEvily, Jr., "Crack Nucleation and Growth in High Strain Low Cycle Fatigue," Trans. of the Metallurgical Society of AIME, Vol 233, pp. 379, Feb. (1968).

7. R. M. Wetzel, "Smooth Specimen Simulation of Fatigue Behavior of Notches," Journal of Materials, Vol. 3, Sept. pp. 646-657 (1968).

8. C. Laird and A. R. Krause, "A Theory of Crack Nucleation in High Strain Fatigue," Scientific Laboratory, Ford Motor Company, Dearborn, Michigan July, (1967).

9. J. H. Crews, Jr., "Local Plastic Stresses in Sheet Aluminum-Alloy Specimens with Stress-Concentration Factor of 2 under Constant-Amplitude Loading," NASA Technical Note, NASA TND-3152, Dec., (1965).

10. G. Rabaut and V. Weiss, "Crack Propagation in Strain Controlled Fatigue," Semi-Annual Report, NASA Contract at Syracuse University, NO. NGR-33-022-023 (1967).

11. W. MacInnes and V. Weiss, "Crack Propagation in Strain Controlled Fatigue," Interim Technical Report, NASA Contract at Syracuse University, NO. NGR-33-022-023, August (1968).

12. H. Neuber, "Theory of Notch Stress: Principles for Exact Stress Calculation," Translated from the German for the David Taylor Model Basin, U. S. Navy, by F. A. Raven, Ph.D. Annotated by J. S. Brock, J. W. Edwards, Ann Arbor Michigan (1946).

13. R. E. Peterson, "Stress Concentration Design Factors," John Wiley and Sons, Inc. (1953).

14. S. S. Manson, "Fatigue: A Complex Subject - Some Simple Approximations," Experimental Mechanics, Vol. 5, No. 7, pp. 193-226 (1965).

15. H. F. Hardrath and L. Ohman, "A Study of Elastic and Plastic Stress Concentration Factors Due to Notches and Fillets in Flat Plates," NACA Report 117 (1953).

16. H. Neuber, "Theory of Stress Concentration for Shear-Strained Prismatic Bodies with Arbitrary Non-Linear Stress-Strain Law," Trans. ASME, Series, E., J. of Applied Mechanics, pp. 544-550. Dec., (1961).

17. H. W. Liu, W. J. Gavigan, K. Lehr, and N. Iino, private communication.

18. H. W. Liu, "Fatigue Crack Propagation and The Stresses and Strains in The Vicinity of A Crack," Applied Materials Research, pp. 229-237, Oct., (1964).

TABLE I

PLASTIC STRAIN DISTRIBUTION UNDER STATIC TENSION OF AM-350 STEEL:

SPEC. NO.	BEFORE LOADING		LOADING CONDITION			AFTER UNLOADING			
	K_t	ρ_o (in.) (mm)	σ_n (ksi) (kg/mm^2)	ε_n	$\varepsilon_p^{ave}+\varepsilon_Y$*	ρ (in.) (mm)	$\varepsilon_{p,NR}$	$K_\varepsilon^n=\frac{\varepsilon_{p,NR}}{\varepsilon_n}$	$K_\varepsilon^{ave}=\frac{\varepsilon_{p,NR}}{\varepsilon_p^{ave}+\varepsilon_Y}$
TU 23	2.0	0.140 (3.56)	104.0 (72.2)	9.0×10^{-2}	6.2×10^{-2}	0.185 (4.70)	140×10^{-2}	1.6	2.2
10	2.6	0.070 (1.78)	91.2 (63.3	7.0×10^{-2}	4.9×10^{-2}	0.093 (2.36	14.5×10^{-2}	2.6	2.9
17	4.0	0.025 (0.635)	81.9 (56.9)	5.4×10^{-2}	4.5×10^{-2}	0.036 (0.91)	18.0×10^{-2}	3.2	3.9
15	4.0	0.025 (0.635)	----	----	----	0.045 (1.14)	28.0×10^{-2}	---	---
15	4.0	0.025 (0.635)	----	----	----	0.31 (0.79)	11.0×10^{-2}	---	---
13	6.0	0.010 (0.25)	79.3 (55.1)	4.4×10^{-2}	3.7×10^{-2}	0.015 (0.38)	21.0×10^{-2}	5.0	5.5

*$\varepsilon_Y = 2 \times 10^{-3}$; obtained from the strain corresponding to the elastic limit.

TABLE I (con't.)

SPEC. NO.	BEFORE LOADING		LOADING CONDITION			AFTER UNLOADING			
	K_t	ρ_o (in.) (mm)	σ_n (ksi) (kg/mm^2)	ε_n	$\varepsilon_p^{ave}+\varepsilon_Y$	ρ (in.) (mm)	$\varepsilon_{p,NR}$	$K_\varepsilon^n=\frac{\varepsilon_{p,NR}}{\varepsilon_n}$	$K_\varepsilon^{ave}=\frac{\varepsilon_{p,NR}}{\varepsilon^{ave}+\varepsilon_Y}$
TU_{12}	6.0	0.010 (0.25)	----	----	----	0.0185 (0.470)	28.0×10^{-2}	----	----
12	6.0	0.010 (0.25)	----	----	----	0.0140 (0.356)	14.0×10^{-2}	----	----
12	6.0	0.010 (0.25)	----	----	----	0.0120 (0.305)	8.0×10^{-2}	----	----
12	6.0	0.010 (0.25)	----	----	----	0.0175 (0.445)	26.0×10^{-2}	----	----
9	8.3	0.005 (0.127)	----	----	----	0.0115 (0.292)	36.0×10^{-2}	----	----
8	8.3	0.005 (0.127)	77.0 (53.5)	3.3×10^{-2}	3.1×10^{-2}	0.0080 (0.203)	22.0×10^{-2}	6.7	7.0
3	12.5	0.002 (0.0051)	75.6 (52.5)	3.1×10^{-2}	2.9×10^{-2}	0.0045 (0.114)	37.0×10^{-2}	12.0	12.5
1	12.5	0.002 (0.051)	----	----	----	0.0057 (0.145)	43.0×10^{-2}	----	----

TABLE II

CHEMICAL AND MECHANICAL PROPERTIES OF

THE ALUMINUM ALLOY 7075-T6

CHEMICAL COMPOSITION:

ELEMENTS	PERCENTS MINIMUM	MAXIMUM
COPPER	1.2	2.0
MAGNESIUM	2.1	2.9
MANGANESE	---	0.30
IRON	---	0.7
SILICON	---	0.5
ZINC	5.1	6.1
CHROMIUM	0.18	0.40
TITANIUM	---	0.20
OTHER IMPURITIES		
EACH	---	0.05
TOTAL	---	0.15
ALUMINUM	BALANCE	

MECHANICAL PROPERTIES:

ULTIMATE STRENGTH	95 ksi (66.0 kg/mm^2)
YIELD STRENGTH (0.2% proof)	68 ksi (47.2 kg/mm^2)
REDUCTION OF AREA	40 %
YOUNG'S MODULUS	10,400 ksi (7221.8 kg/mm^2)

TABLE III

FATIGUE CRACK INITIATION DATA OF 7075-T6 ALUMINUM

SERIES NO.	ρ (in.) (mm)	K_t	ε^{tr}	$\varepsilon^{tr}_{NR} = \ln\sqrt{\frac{\rho_T}{\rho_C}}$	$\frac{W_p}{\sigma_Y \rho^2 t}$	ΔP^{tr} (lb.) (kg)	N_o	$\varepsilon^{tr}_{p,NR}$
A-1	0.06 (1.52)	2	3×10^{-2}	6.1×10^{-2}	1.8×10^{-1}	11,450 (5193.7)	24	4.14×10^{-2}
A-2	0.06 (1.52)	2	1.7×10^{-2}	3.0×10^{-2}	1.1×10^{-2}	8,300 (3764.9)	200	1.14×10^{-2}
A-3	0.06 (1.52)	2	1.7×10^{-2}	2.8×10^{-2}	9.0×10^{-3}	8,440 (3828.4)	180	0.96×10^{-2}
A-5	0.06 (1.52)	2	2.3×10^{-2}	5.2×10^{-2}	1.2×10^{-1}	11,330 (5139.3)	36	3.34×10^{-2}
A-11	0.06 (1.52)	2	2.3×10^{-2}	5.3×10^{-2}	1.3×10^{-1}	11,800 (5352.5)	25	3.44×10^{-2}
B-1	0.02 (0.51)	3	1.0×10^{-2}	3.4×10^{-2}	2.2×10^{-2}	5,540 (2512.9)	300	1.28×10^{-2}
B-2	0.02 (0.51)	3	2.3×10^{-2}	---	8.3×10^{-1}	11,300 (5125.7)	10	---
B-3	0.02 (0.51)	3	1.7×10^{-2}	---	1.4×10^{-1}	8,530 (3869.2)	60	---

TABLE III (con't.)

SERIES No.	ρ (in.) (mm)	K_t	ε^{tr}	$\varepsilon^{tr}_{NR} = \ln\sqrt{\frac{\rho_T}{\rho_C}}$	$\frac{W_p}{\sigma_Y \rho^2 t}$	ΔP^{tr} (lb.) (kg)	N_o	$\varepsilon^{tr}_{p,NR}$
B-4	0.02 (0.51)	3	1.7×10^{-2}	5.2×10^{-2}	1.3×10^{-1}	8,500 (3855.6)	58	3.08×10^{-2}
B-5	0.02 (0.51)	3	1.3×10^{-2}	3.9×10^{-2}	4.8×10^{-2}	8,100 (3674.2)	125	1.78×10^{-2}
B-7	0.02 (0.51)	3	2.3×10^{-2}	7.6×10^{-2}	8.2×10^{-1}	11,200 (5080.3)	10	5.48×10^{-2}
C-1	0.01 (0.25)	4	2.7×10^{-2}	---	8.75	12,400 (5624.6)	$N_f = 2\frac{1}{4}$	---
C-2	0.01 (0.25)	4	1.0×10^{-2}	---	6.6×10^{-2}	5,350 (2426.8)	200	---
C-6	0.01 (0.25)	4	1.7×10^{-2}	---	3.8×10^{-1}	8,500 (3855.6)	35	---
C-8	0.01 (0.25)	4	1.0×10^{-2}	3.5×10^{-2}	7.0×10^{-2}	5,500 (2494.8)	280	1.07×10^{-2}
C-9	0.01 (0.25)	4	1.7×10^{-2}	6.8×10^{-2}	5.4×10^{-1}	9,200 (4173.1)	25	4.37×10^{-2}

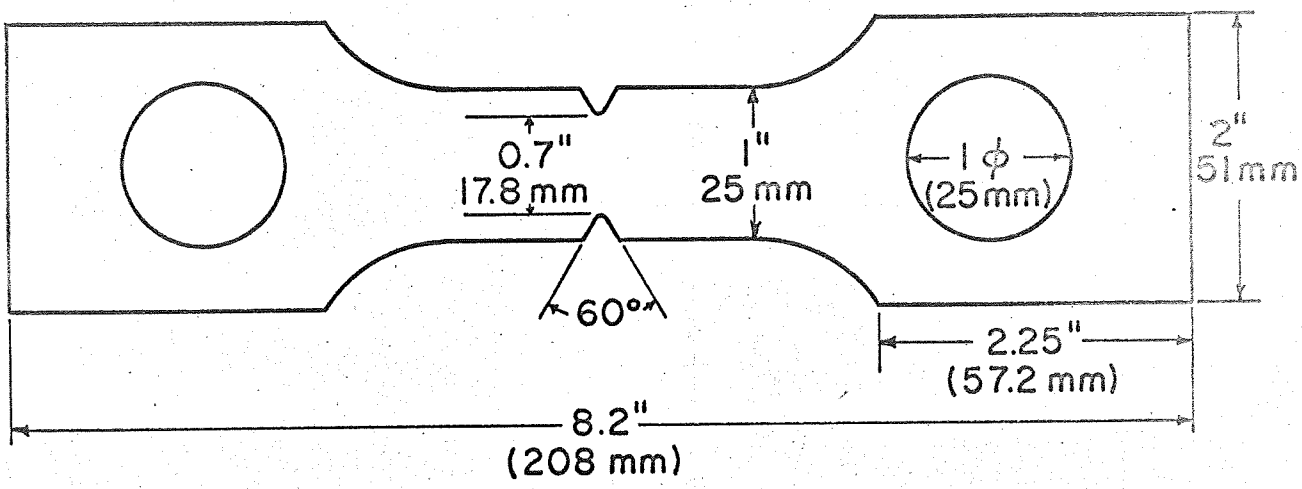

SPECIMEN	TU 23	TU 20	TU 15,17	TU 11,12,13	TU 8,9	TU 1,3
ROOT RADIUS (in) (mm)	0.140 (3.56)	0.070 (1.78)	0.025 (0.64)	0.010 (0.25)	0.005 (0.13)	0.002 (0.05)
K_t VALUE	2.0	2.6	4.0	6.0	8.3	12.5

TU - SPECIMENS ARE TAKEN IN TRANSVERSE TO THE ROLLING DIRECTION.

SPECIMEN THICKNESS: 0.062 inches.

FIGURE 1. GEOMETRY OF AM-350 STEEL SPECIMENS (Fe-17 Cr - 4 Ni - 3 Mo)
σ_Y = 70 ksi (49 kg/mm^2), σ_{TU} = 190 ksi (134 kg/mm^2).

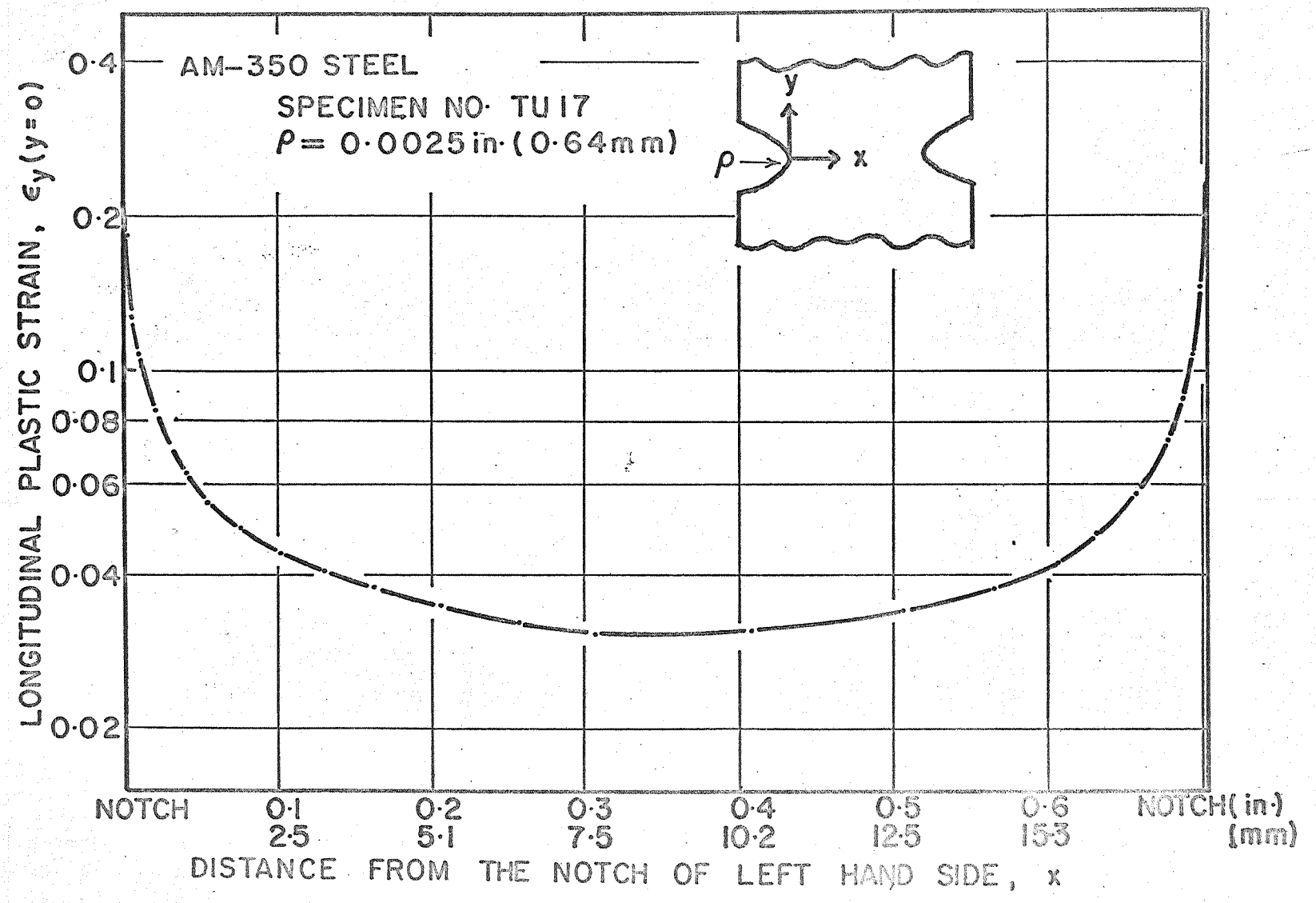

FIGURE 2. STRAIN DISTRIBUTION ACROSS THE NOTCHES AFTER UNLOADING.

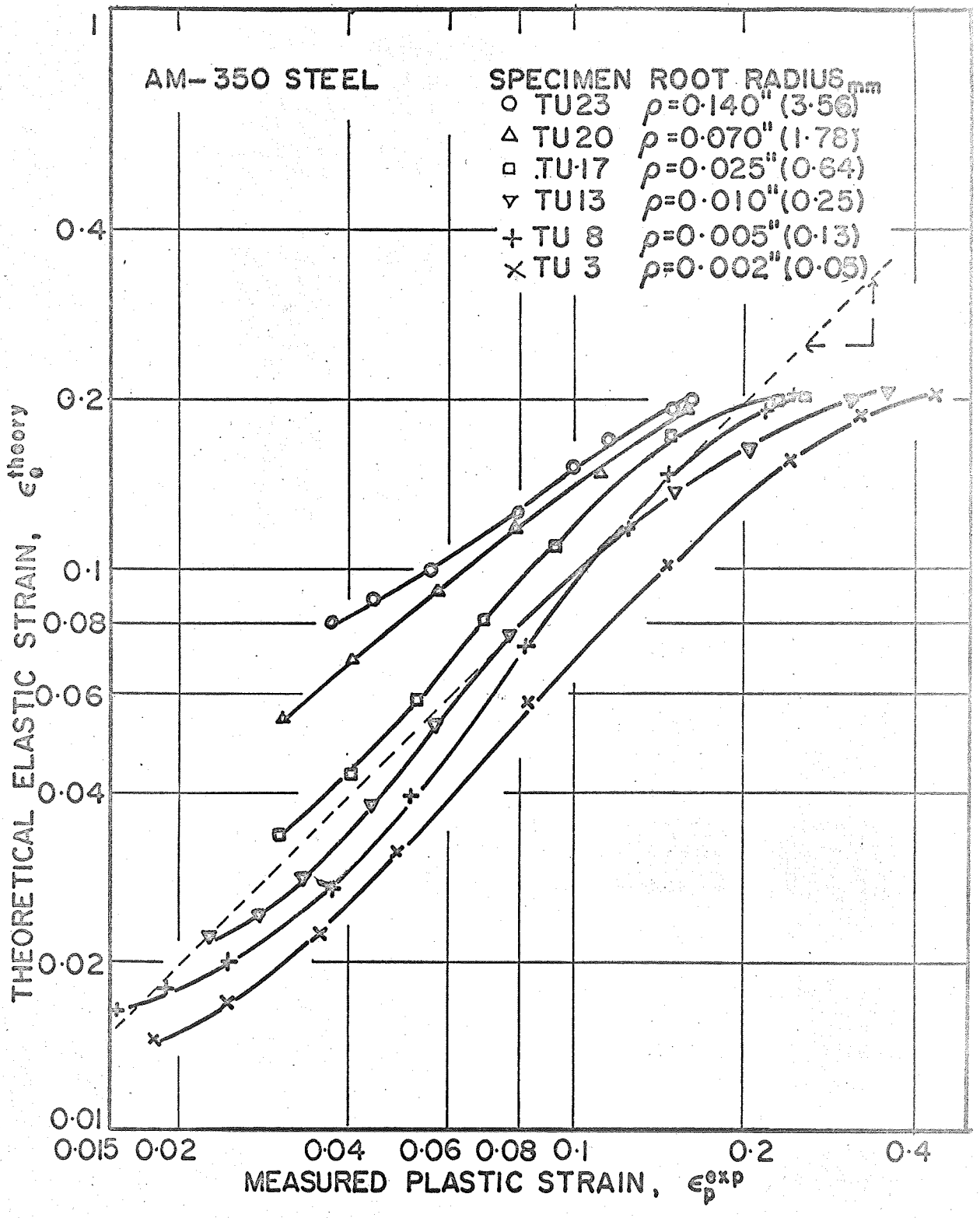

FIGURE 3. COMPARISON OF EXPERIMENTALLY MEASURED PLASTIC STRAIN AFTER UNLOADING AND THE ELASTIC STRAIN PREDICTED FROM NEUBER'S STRESS DISTRIBUTION[13].

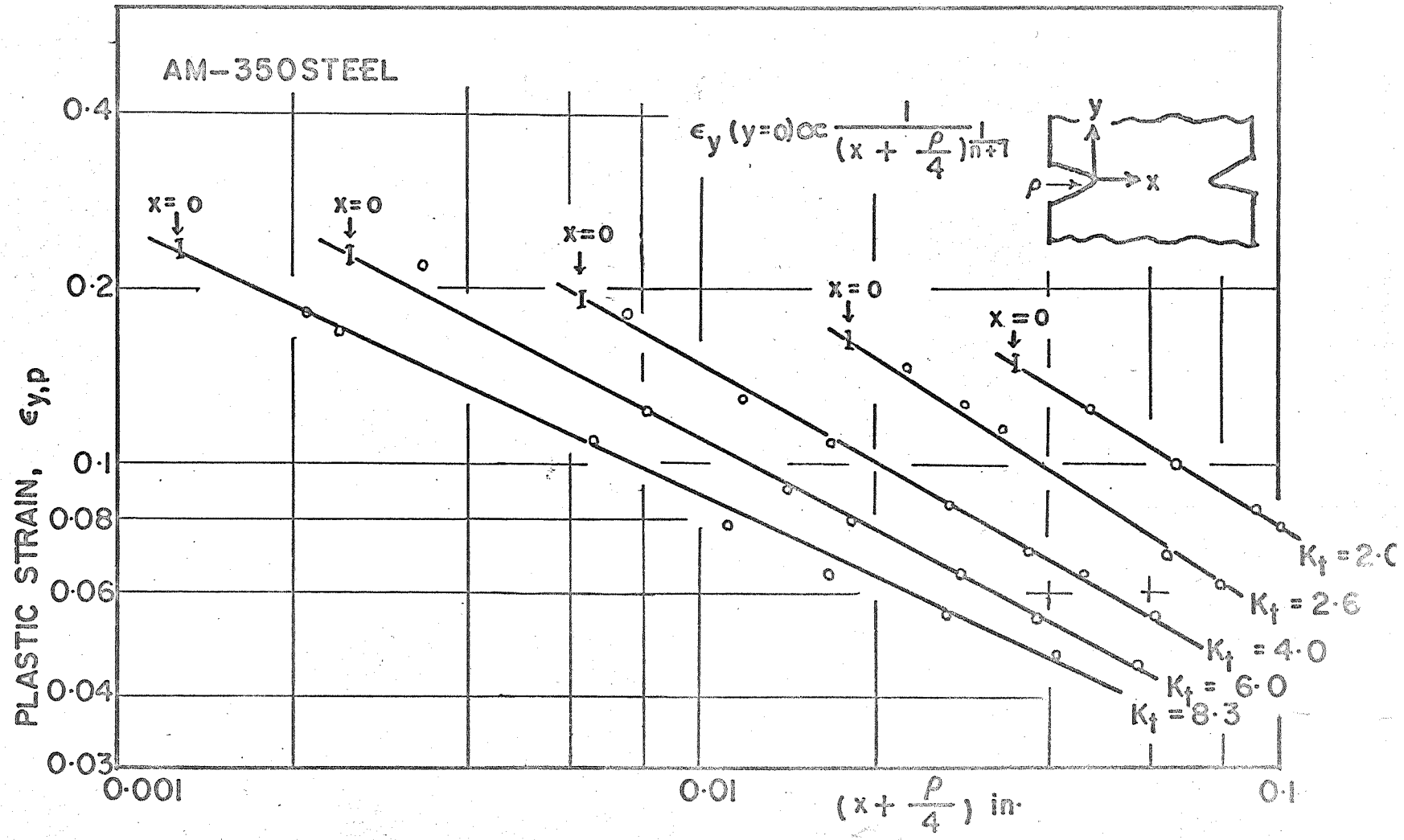

FIGURE 4. DISTRIBUTUION OF THE MAXIMUM PRINCIPAL STRAIN, $\epsilon_y(y=0)$, NEAR THE NOTCH ROOT. PLOT OF $\ln(x + \rho/4)$ VS $\ln \epsilon_y$ ALLOWS EXTRAPOLATION TO $x = 0$, I.E. THE DETERMINATION OF $\epsilon_{y,NR}$ AT THE NOTCH ROOT.

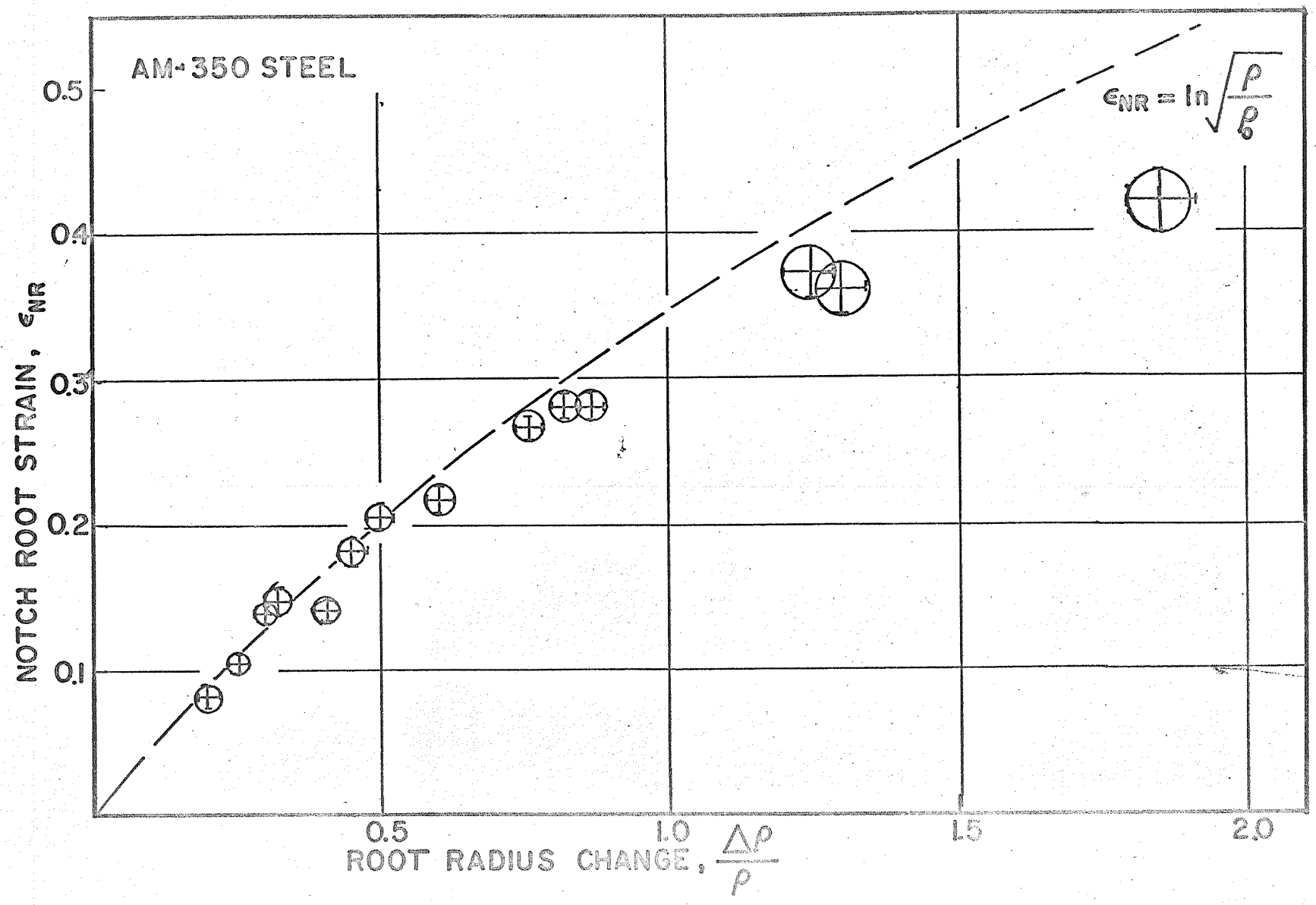

FIGURE 5. RELATIONSHIP BETWEEN ROOT RADIUS CHANGE AND MAXIMUM STRAIN AT NOTCH ROOTS.

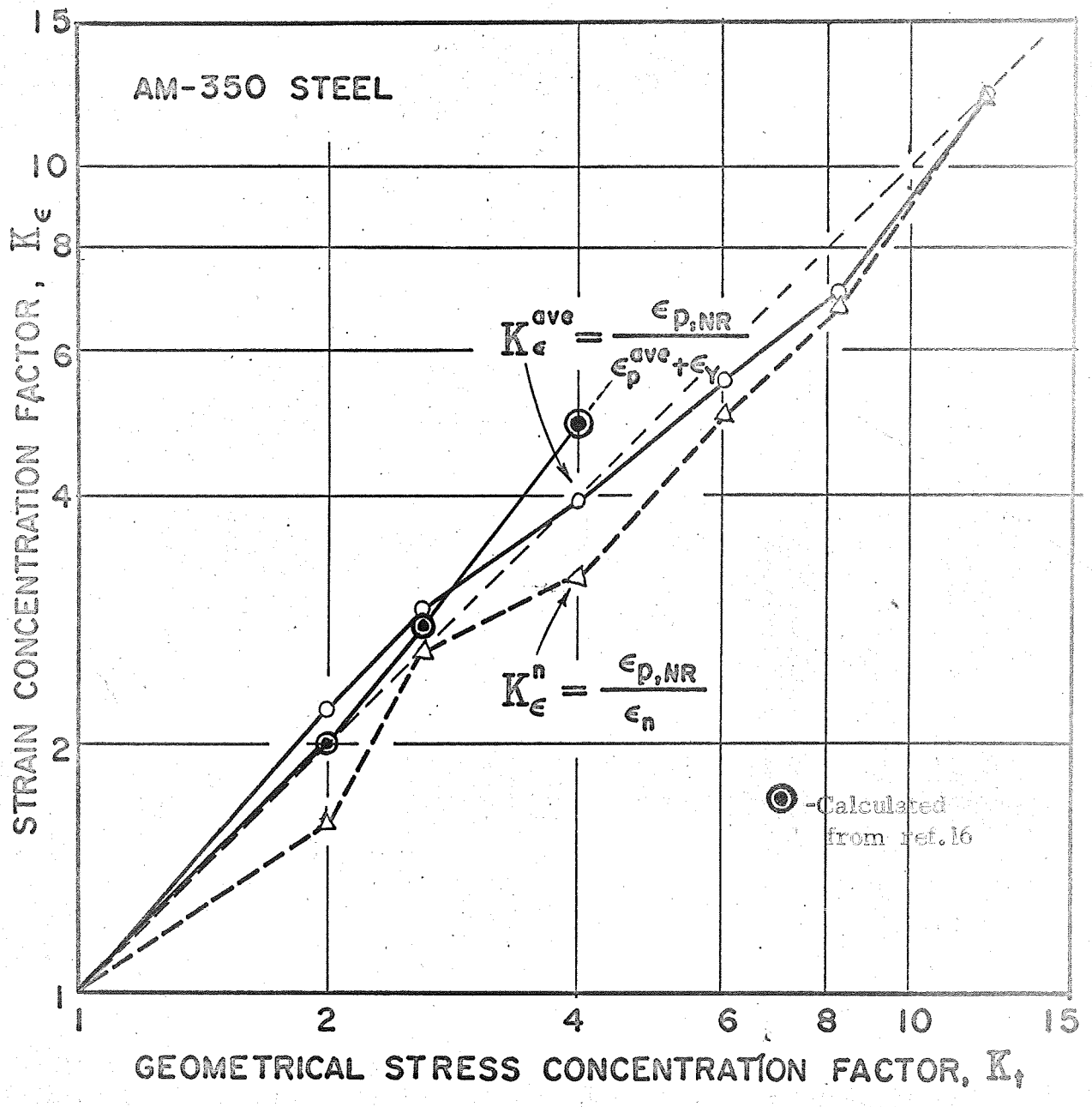

FIGURE 6. STRAIN CONCENTRATION FACTOR AS A FUNCTION OF GEOMETRIC ELASTIC STRESS CONCENTRATION FACTOR.

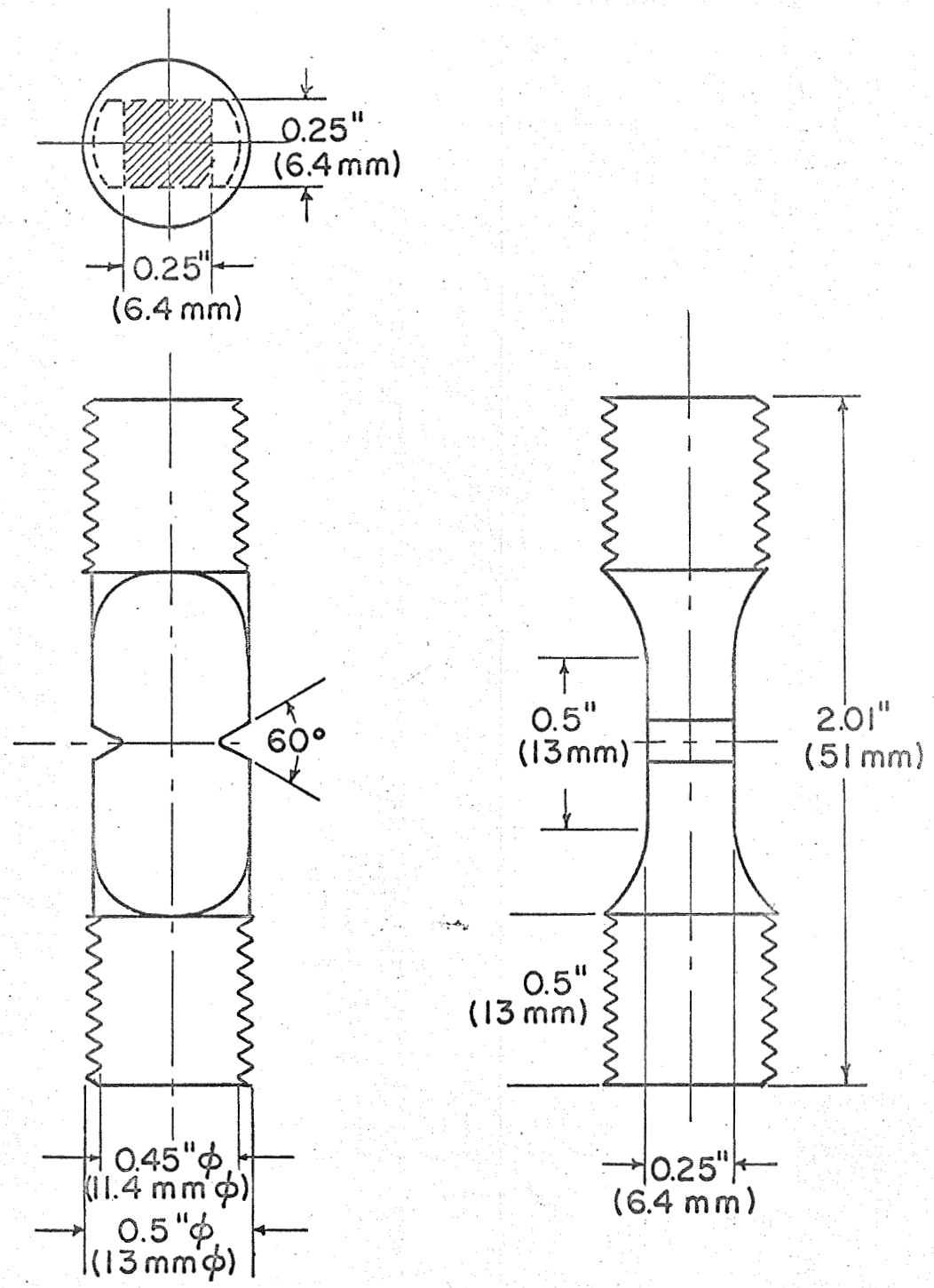

SERIES	A	B	C
ROOT-RADIUS (in) (mm)	0.06 1.52	0.02 0.51	0.01 0.25
K_t VALUE	2	3	4

FIGURE 7. LOW CYCLE FATIGUE TEST SPECIMAN, Al 7075-T6.

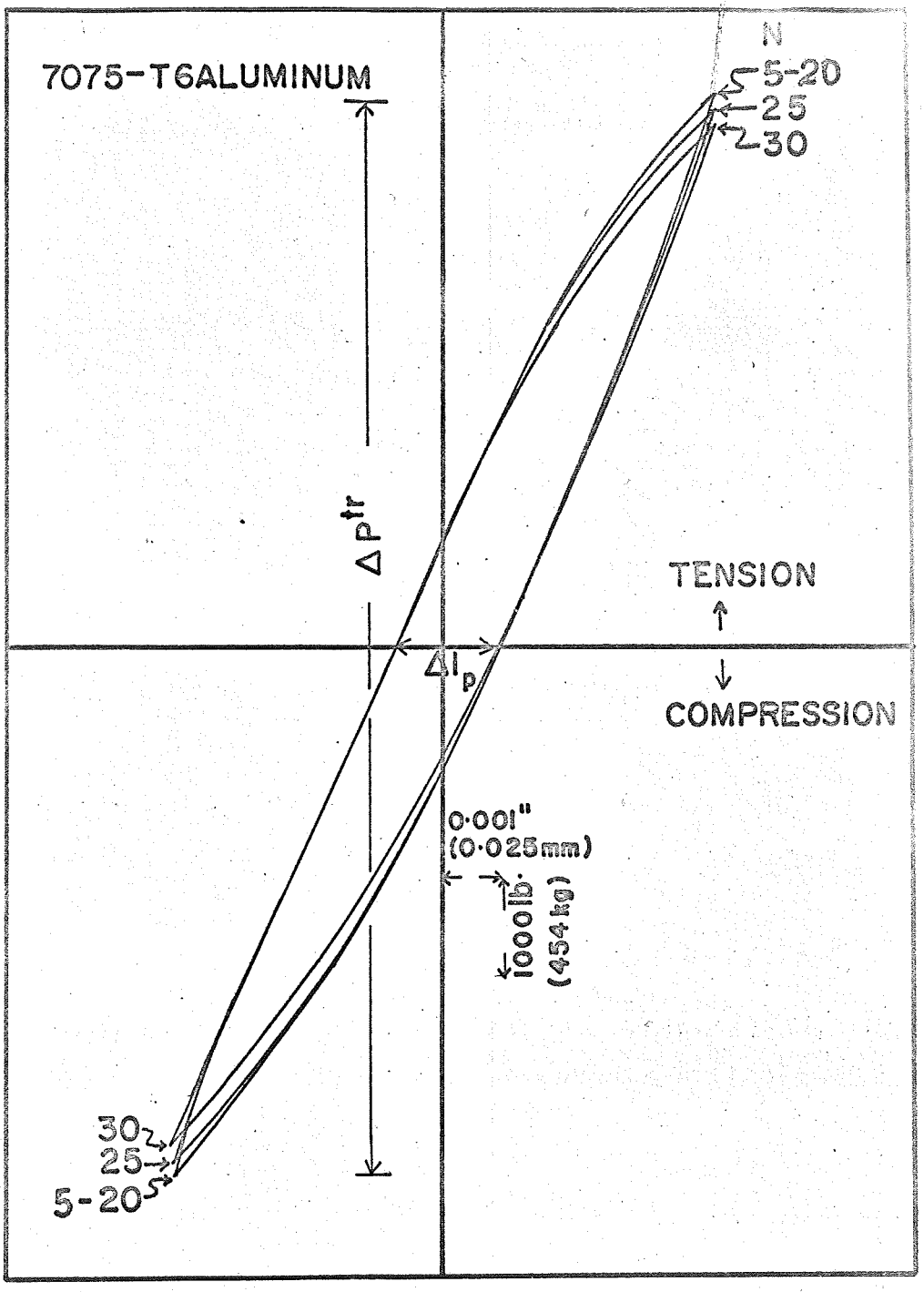

FIGURE 8. TYPICAL HYSTERESIS CURVE OF 7075-T6

$\varepsilon_p^{tr} = 6.3 \times 10^{-3}$, $\varepsilon^{tr} = 3 \times 10^{-2}$

$\varepsilon_{NR}^{tr} = 6.1 \times 10^{-2}$, $N_o = 25$

GAUGE LENGTH 0.300 in. (7.6 mm).

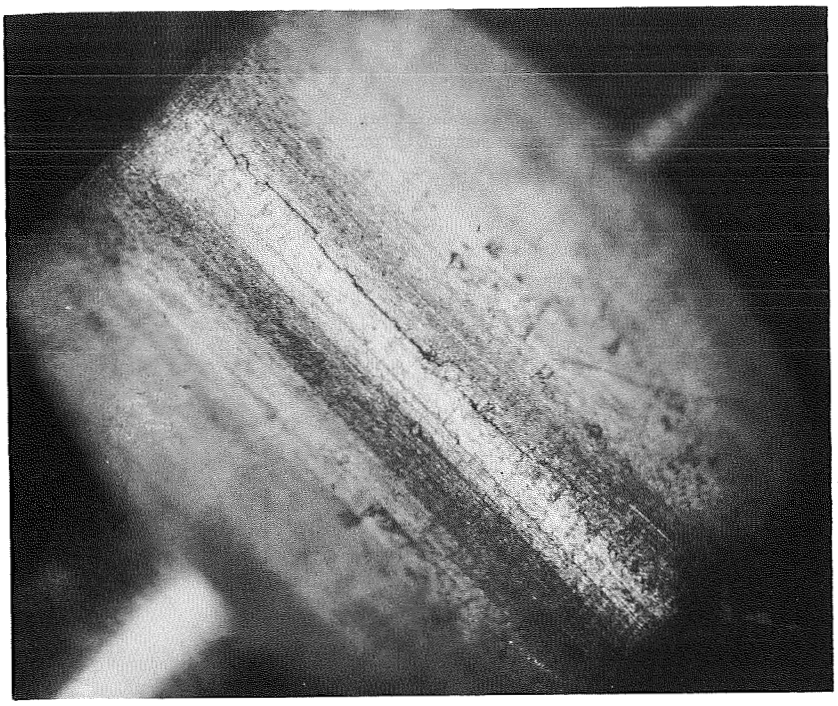

15x (C)

SUB-
CRACKS
(STAGE-I)

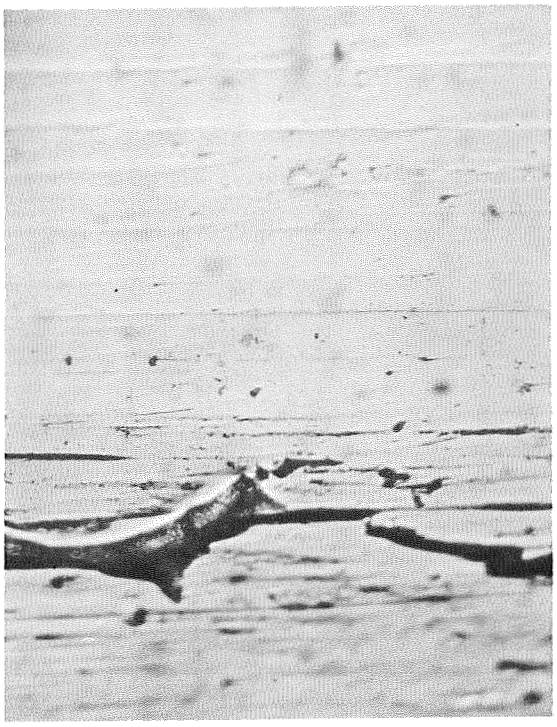

MAIN CRACK
(STAGE-II)

500x (D)

FIG. 9 NOTCH ROOT OF A-2 SPECIMEN
(AFTER CRACK INITIATION)
$K_t = 2$: $N_o = 200$: $\rho = 0.06$ in.
(1.5 mm)

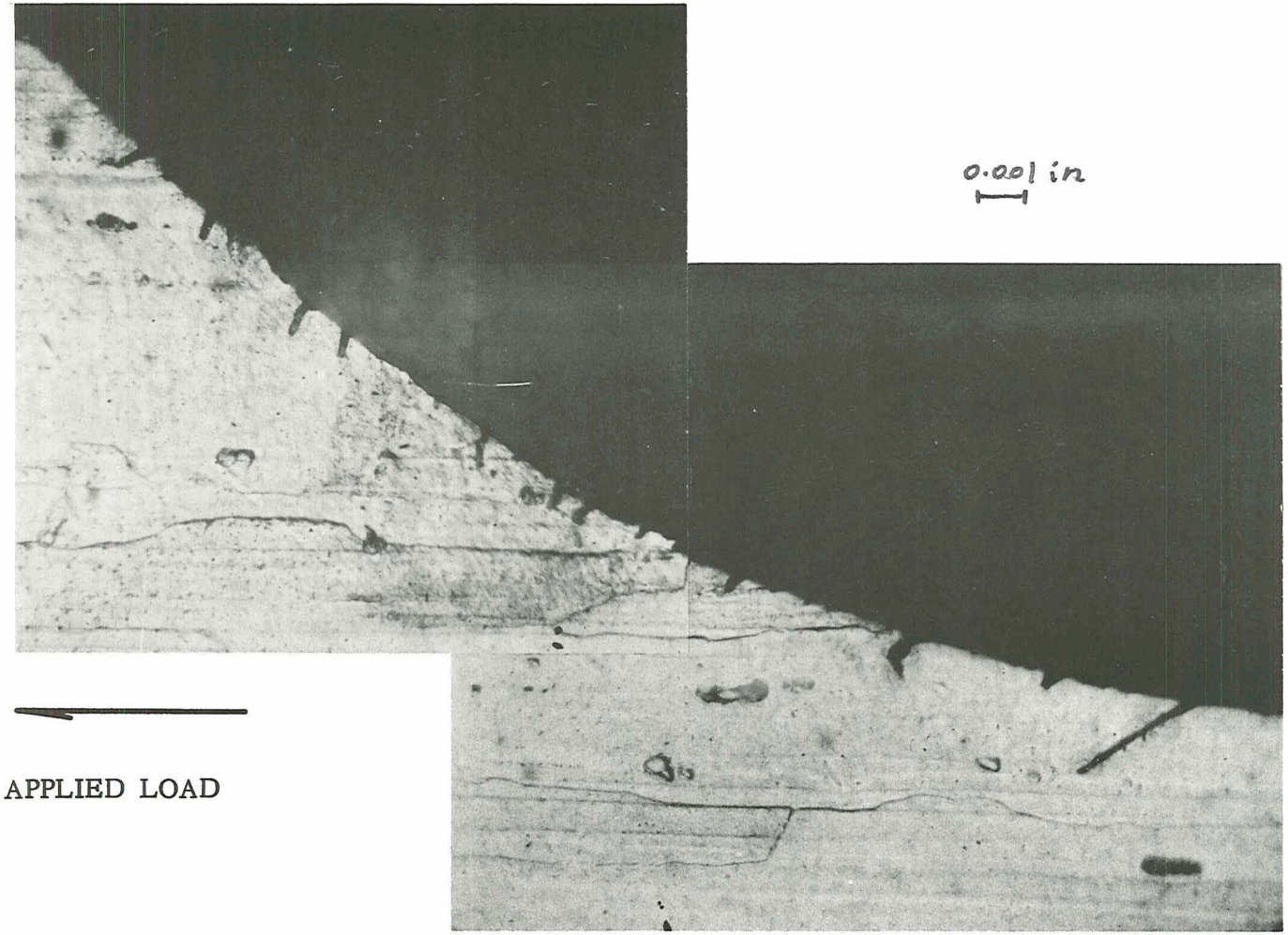

FIG.10 STAGE-I MICROCRACKS AT THE NOTCH ROOT OF 7075-T6 ALUMINUM
(ETCHED WITH KELLER'S ETCHANT)

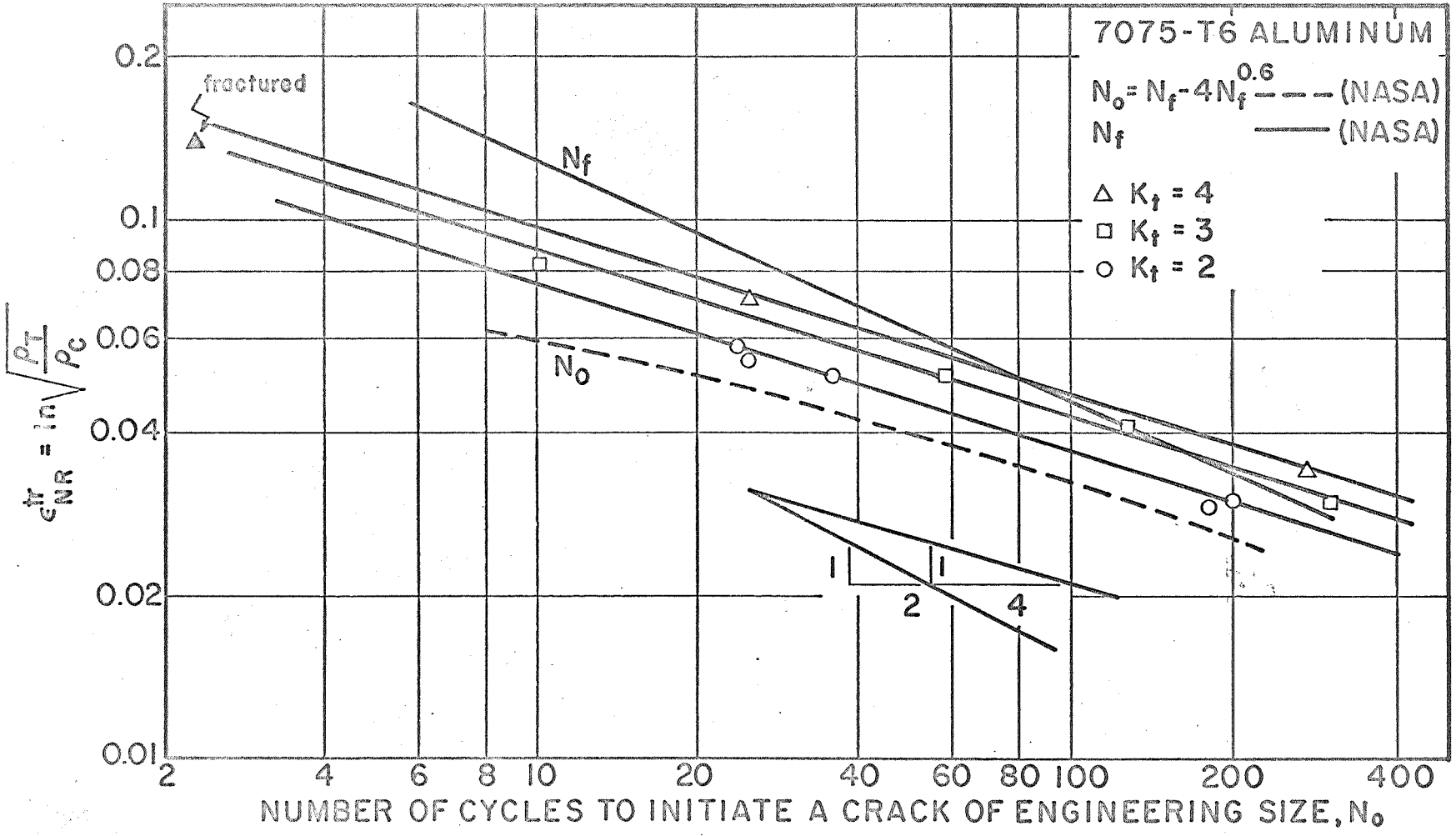

FIGURE 11. EFFECT OF TOTAL STRAIN RANGE AT THE NOTCH ROOT ON THE NUMBER OF CYCLES TO INITIATE A CRACK OF ENGINEERING SIZE, 5×10^{-3} to 10^{-2} in. (0.1 to 0.3 mm).

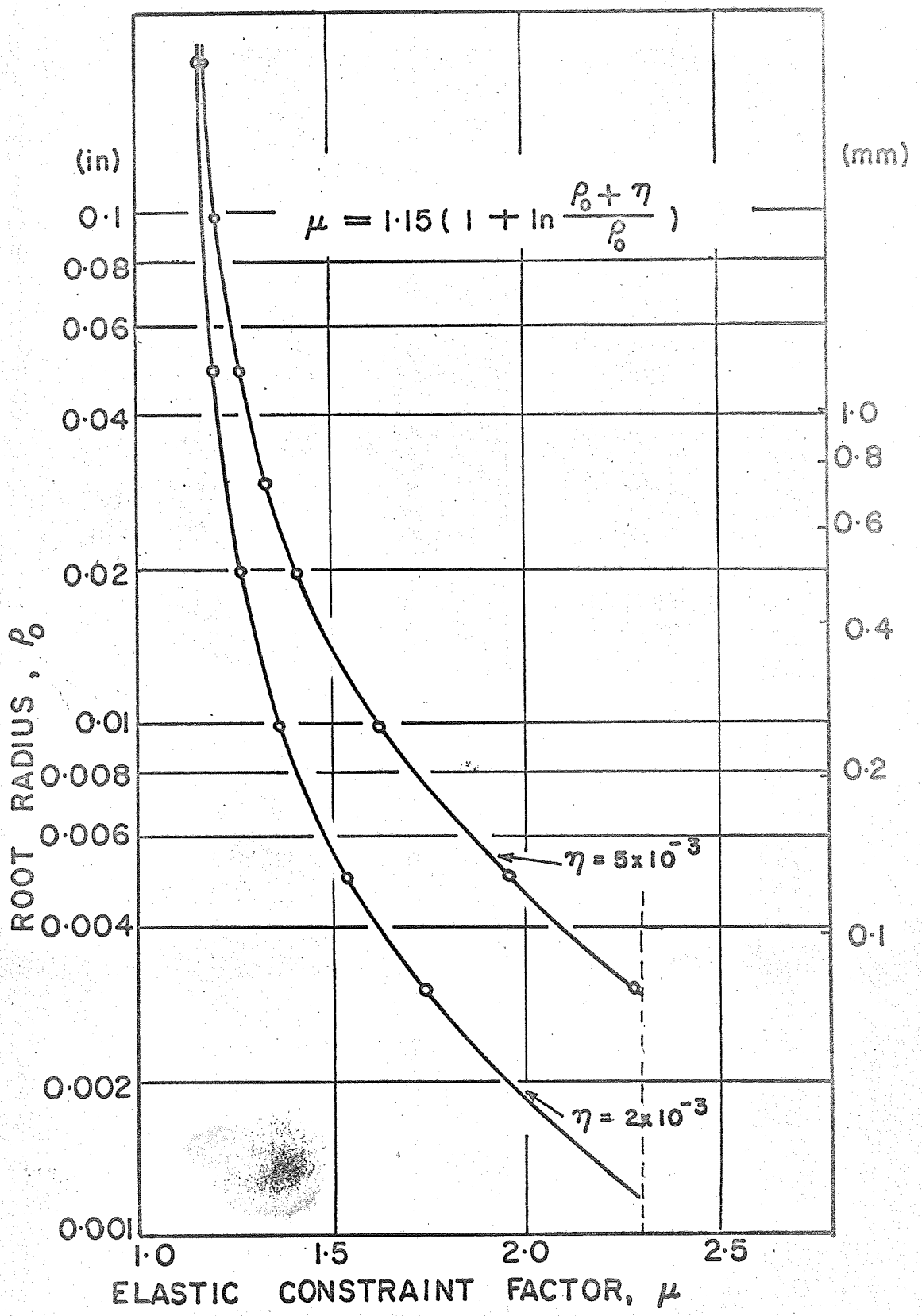

FIGURE 12. EFFECT OF ROOT RADIUS ON THE CONSTRAINT FACTOR (η: PARAMETER).

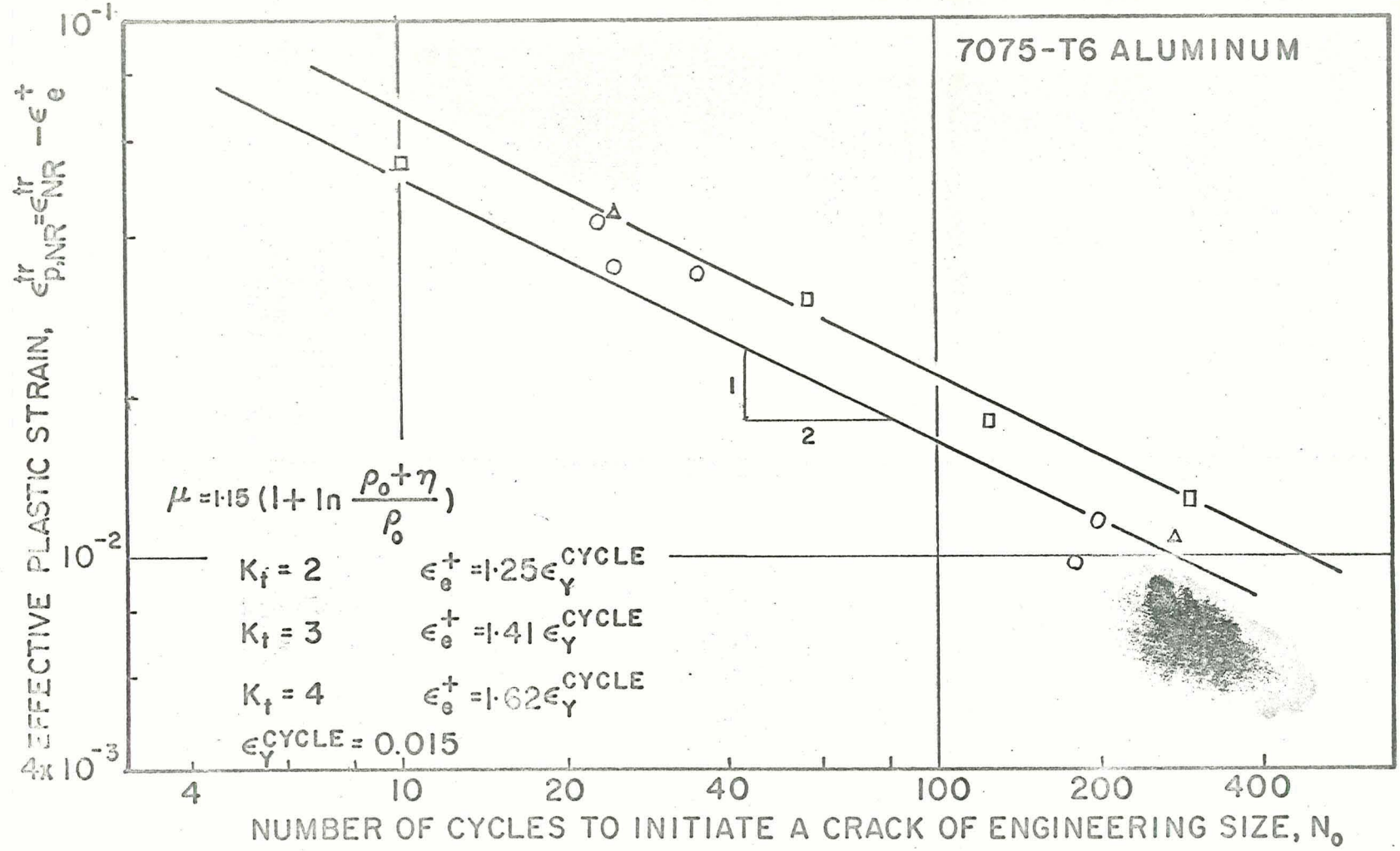

FIGURE 13. EFFECTIVE PLASTIC STRAIN RANGE VS. NUMBER OF CYCLES TO INITIATE A CRACK OF ENGINEERING SIZE, N_o.

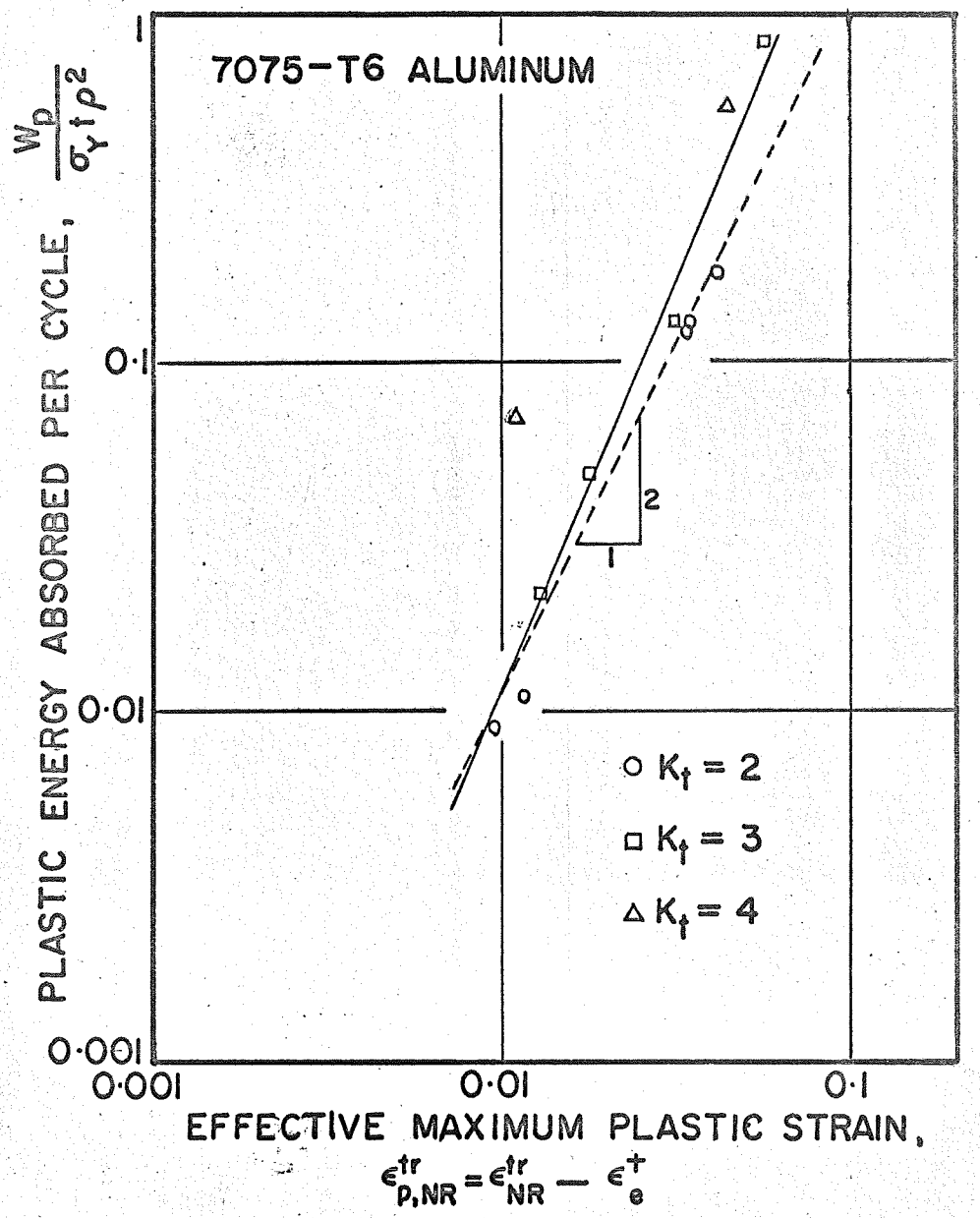

FIGURE 14. RELATIONSHIP BETWEEN PLASTIC ENERGY ABSORPTION PER CYCLE AND EFFECTIVE MAXIMUM STRAIN AT THE NOTCH ROOT.

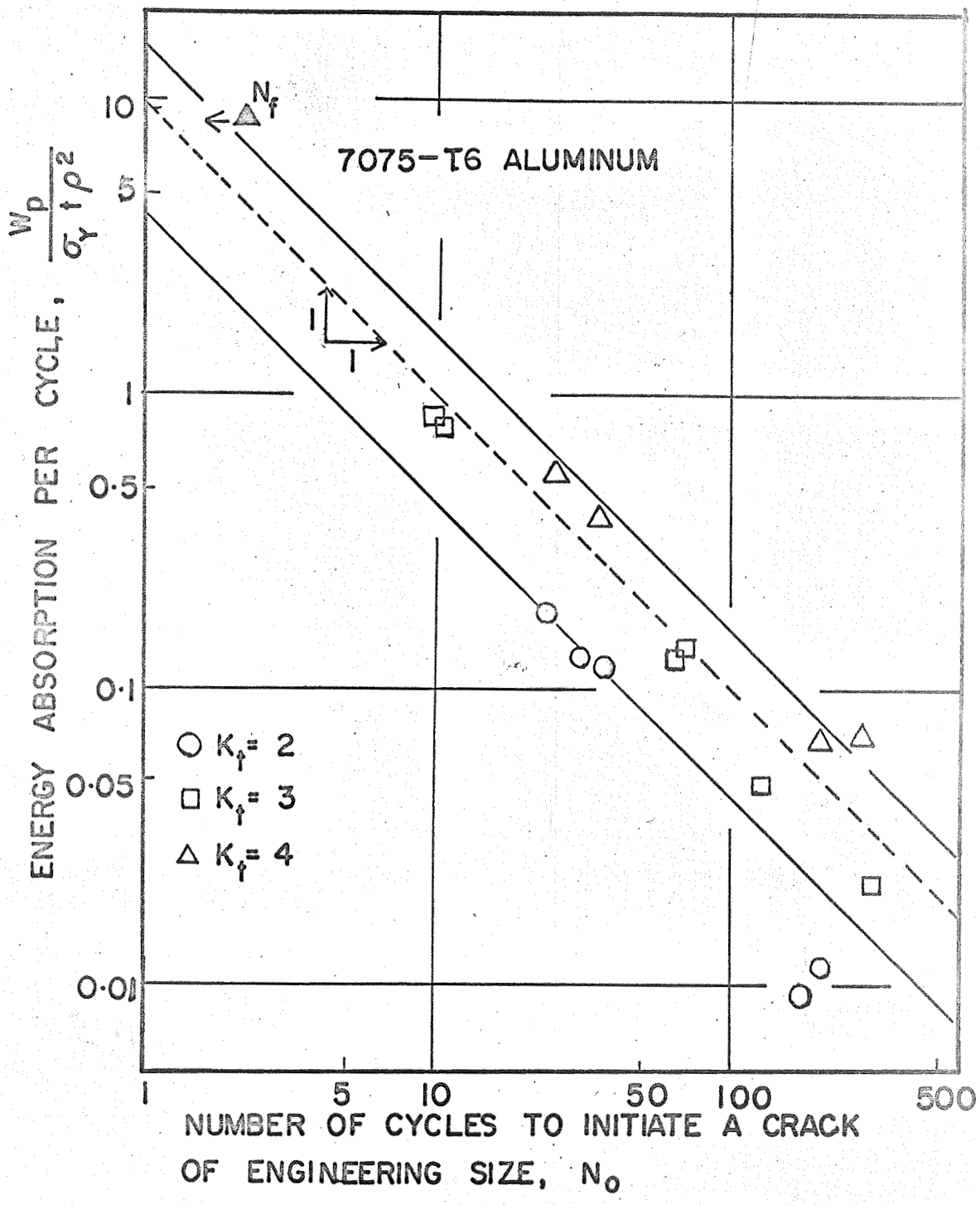

FIGURE 15. RELATIONSHIP BETWEEN PLASTIC ENERGY ABSORBED PER CYCLE AND THE NUMBER OF CYCLES TO CRACK INITIATION.

CRACK PROPAGATION AND INITIATION IN LOW CYCLE STRAIN CONTROLLED FATIGUE*)

V. Weiss, G. Rabaut, W. MacInnes

*Department of Chemical Engineering and Metallurgy, Syracuse University, Syracuse***)*

Experimental techniques for crack extension measurements in cylindrical specimens, subjected to tension-compression strain cycling, are described. Both electrical resistivity and compliance techniques are applicable and yield information on crack growth as well as crack initiation.

Crack propagation follows the relationship

$$\mathrm{d}c/\mathrm{d}N = A \,.\, c \,.\, (\varepsilon_{TR}/\varepsilon_F)^{n+1} - \frac{\varrho^*}{2}$$

with n close to unity. (Here c is the crack length, A a constant and ε_F a critical strain characteristic of the material; ε_{TR} is the total strain range.) The Manson-Coffin equation could be regarded as a consequence of this crack propagation relationship, though the value of the strain hardening exponent $n \simeq 1$ will require further verification and clarification.

From preliminary tests it appears that crack initiation in notched specimens is also governed by a Manson-Coffin type relationship, especially if the effective plastic strain at the notch root can be properly computed from

$$\varepsilon_{TR,\,\mathrm{effective}} = K_\varepsilon \cdot \varepsilon_{TR} - \varepsilon_e^+$$

where K_ε is the proper strain concentration factor, ε_{TR} the total nominal strain range and ε_e^+ the elastic component under consideration of the plastic constraint at the notch root.

1. INTRODUCTION

The search for mechanisms responsible for fatigue might appear particularly promising for the field of high amplitude, strain controlled low cycle fatigue; first, because the suspected damage process could be easily followed from cycle to cycle and second, because of the good agreement of the results for most metals and alloys with the Manson-Coffin relationship [1, 2], so that any mechanism proposed must necessarily be in agreement with the Manson-Coffin law. This well known relationship states that

$$N_f^a \varepsilon_p = \text{const.} \tag{1}$$

where N_f is the number of cycles to failure, a approximately 0·5 to 0·6 and ε_p the plastic strain range. The constant on the right-hand side of Eq. 1 has the character of a strain and has been related to the tensile fracture strain. It is a material constant and represents the strain value ε_p extrapolated according to the Manson-Coffin relationship to $N_f = 1/4$ cycle and will be referred to as ε_F^* in the following [3]. The

*) The work reported here was sponsored by the U. S. National Aeronautics and Space Administration, Grant No. NGR-33-022-023. The authors gratefully acknowledge the continued interest and support given by Mr. S. S. Manson of NASA's Lewis Research Center, Cleveland, Ohio.

**) *Syracuse, N.Y. 13210, U.S.A.*

agreement of ε_F^* with the tensile fracture strain varies strongly from material to material [4]. Thus equation (1) may be regarded as a summation rule for the damage with failure occurring when a critical value $\varepsilon_{F_1}^*$, the low cycle fatigue fracture strain, is reached, i.e. low cycle fatigue might be regarded as a case of cumulative strain exhaustion.

This argument was further supported by the experimental results of the effects of mean strain or pre-strain. In strain controlled fatigue, mean strain is synonymous to

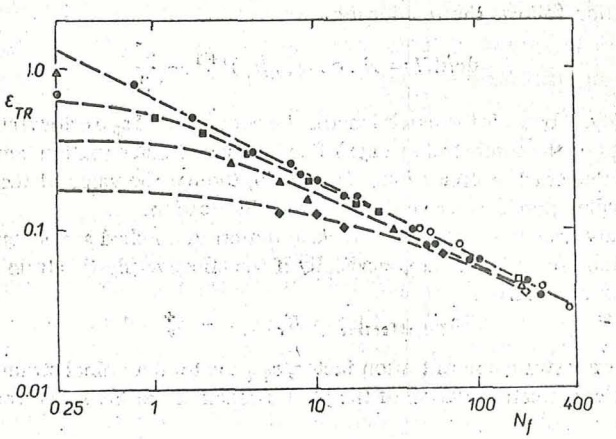

Fig. 1. Comparison of strain cycling experimental results for A 302 and A 225 steels with theoretical curves derived from equation 2 using ε_{TR} instead of ε_p as the elastic component is small. *Monotonic tension* ε_F: ⊙ — A 302, △ — A 225.

R	A 302	A 225
0·75	◆	◊
0·50	▲	△
0	■	□
−1	●	○

Dashed lines according to:

$$N_f = [\varepsilon_F^* - \varepsilon_0/\varepsilon_{TR}]^{1/a} \quad a = 1/2\,. \tag{1}$$

pre-strain since there is no difference between cycling with ε_p around a mean strain ε_0 or prestraining first to ε_0 and then cycling symmetrically between $\pm\varepsilon_p/2$. The experimental data are in excellent agreement with the relationship

$$N_f^a \varepsilon_p = \varepsilon_F^* - \varepsilon_0 \tag{2}$$

i.e. the low cycle fatigue fracture strain is reduced by the amount of the mean or pre-strain, as illustrated in Fig. 1 [3].

The hypothesis of strain exhaustion was tested more directly by measuring the remaining tensile fracture strain, ε_{FR}, after strain cycling for N_x cycles, $N_x < N_f$.

According to equation (1), the remaining tensile fracture strain should be given by

$$\varepsilon_{FR} = \varepsilon_F^*[1 - (N_x/N_f)^\alpha] . \tag{3}$$

The experimental results, however, as shown for two steels in Figs. 2 and 3, are in definite disagreement with the predictions of Eq. (3), i.e. with the strain exhaustion hypothesis. While some loss in fracture strain with increasing N_x values is observed

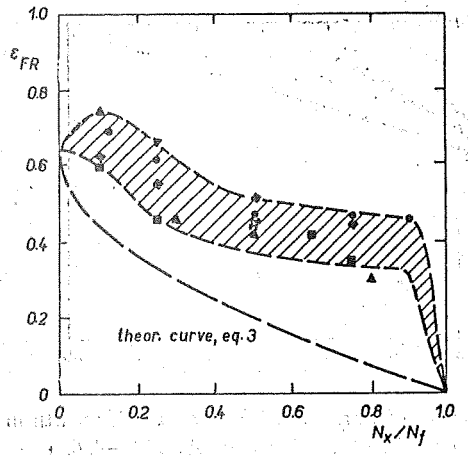

Fig. 2. Comparison of measured ε_{FR} after strain-cycling to N_x cycles to that predicted by Eq. (3) for A 302 steel. $\varepsilon_F^* = 0{\cdot}64$, $R = -1$; ▼ – $\varepsilon_{TR} = 0{\cdot}300$, ▲ – $\varepsilon_{TR} = 0{\cdot}200$, ■ – $\varepsilon_{TR} = 0{\cdot}140$, ● – $\varepsilon_{TR} = 0{\cdot}100$, ♦ – $\varepsilon_{TR} = 0{\cdot}064$.

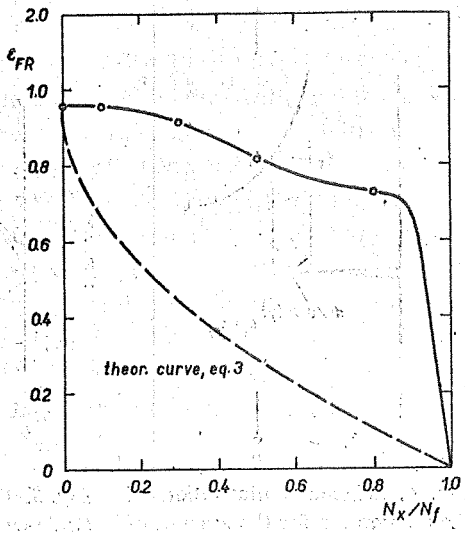

Fig. 3. Comparison of measured ε_{FR} after strain-cycling to N_x cycles to that predicted by Eq. (3) for A 225 steel.

the experimental results do not at all follow the trend of the curve (dashed line) predicted by Eq. (3). Thus, strain exhaustion alone cannot be the major damage mechanism. Tensile tests at −320F on steels after partial cycling at room temperature showed a loss in strength with increasing N_x values, which was suggestive of crack formation and propagation as another damage mechanism.

To guide the experimental program on crack propagation and initiation in low cycle strain controlled fatigue an estimate of the expected crack propagation behavior was made by Weiss [5] on the basis of notch analysis of fracture [6]. The central assumption of this estimate is that the incremental crack growth per cycle will be equal to the distance over which the strain ahead of an existing crack (length c) exceeds some critical value, ε_{FF}. With the help of Neuber's rule [7] for stress and strain concentration factors K_σ, K_ε, in the non-linear range

$$K_\sigma \cdot K_\varepsilon = K_t^2 \tag{4}$$

where K_t is the elastic theoretical or Hookeian stress concentration factor and an assumption for the stress strain relationship, the plastic stress and strain distribution near the tip of a crack can be obtained from the elastic distribution. The elastic stress distribution near the tip of a crack is given by

$$\sigma_y = \sigma_N \left(\frac{2c}{\varrho^* + 2x} \right)^{1/2} \tag{5}$$

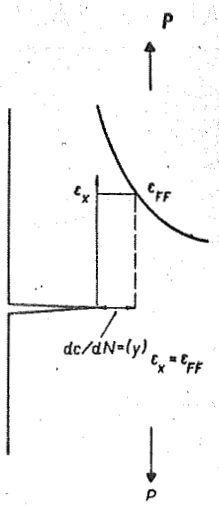

Fig. 4. Schematic illustration of the assumption for the amount of incremental fatigue crack growth.

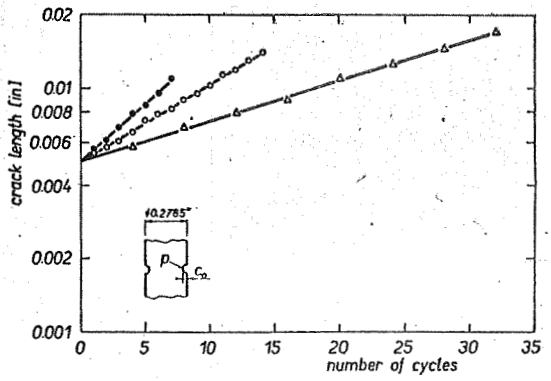

Fig. 5. The effect of strain amplitude on crack growth in strain-cycled cylindrical specimens of Al 7075—T6. ● — $\varepsilon_{TR} = 0{\cdot}0374$, ○ — $\varepsilon_{TR} = 0{\cdot}0274$, △ — $\varepsilon_{TR} = 0{\cdot}0147$. Circumferentially notched round specimens $K_t = 3{\cdot}5$, $\varrho = 0{\cdot}003''$, $c_0 = 0{\cdot}005''$.

where x is the distance from the crack tip, ϱ^* the microsupport effect for sharp notches and σ_N the net section stress cf. Fig. 4. [8]. The assumption of an exponential stress strain law

$$\sigma = k\varepsilon^n \tag{6}$$

is convenient for the estimate, however it must be emphasized that one must consider total stress and strain, not just their elastic components, and that the constants k and n should be fitted to the fatigue stress strain curve under the multiaxial stress state, characteristic for the vicinity of a crack. Thus one obtains for the strain distribution near the crack tip

$$\varepsilon_y = \varepsilon_N \left(\frac{2c}{\varrho^* + 2x} \right)^{1/(n+1)} \tag{7}$$

and the incremental crack growth in accordance with the above assumptions

$$\frac{\mathrm{d}c}{\mathrm{d}N} = \frac{c}{2} \cdot \left(\frac{\varepsilon_{TR}}{\varepsilon_{FF}} \right)^{n+1} - \frac{\varrho^*}{2} . \tag{8}$$

For the elastic case $n = 1$, $\sigma = E\varepsilon$, this is in agreement with Liu's analysis [9] according to which $dc/dN = A \cdot K^2$, where K is the stress intensity factor (for the present geometry $K = \sigma(\pi c)^{1/2}$), and π a constant. Accordingly, a plot of $\ln c$ vs. N should yield straight lines. This is certainly indicated in the results shown in Fig. 5. Furthermore, Eq. (8) can be integrated and yields

$$N_f \varepsilon_{TR}^{(n+1)} = \text{const.} \tag{9}$$

which is identical with the Manson-Coffin relationship if $n = 0{\cdot}66$ to 1; this high value of the apparent strain hardening exponent will require further clarification.

The above presented experimental evidence in combination with notch analysis was deemed sufficient to warrant a further, more detailed study of the characteristics of crack propagation and initiation in strain controlled low cycle fatigue. Tension-compression cycling with zero mean strain was chosen to avoid the complications involved in bend cycling. A1 7075 T6 was selected because previous experiments [4] have shown this material to be neither strain hardening nor strain softening. The main experimental challenge was to develop a reliable non-destructive method for monitoring the crack length as a function of the number of cycles. The elastic compliance and the electrical resistivity methods chosen also allowed some preliminary observations on crack initiation at the base of shallow circumferential notches.

2. EXPERIMENTAL

The test specimen and schematic representations of the crack length measuring techniques utilized are shown in Figs. 6 and 7. For the present study the electrical resistance and the compliance (the reciprocal of the spring constant), were selected for determining crack initiation and following crack propagation non-destructively.

The electrical potential technique, Fig. 6, utilizes the potential drop between two fixed locations on the specimen, above and below the crack[1]), see insert Fig. 6a. The relationship between potential change and crack depth was determined empirically, cf. calibration curve, Fig. 6b. In this calibration, the various crack depths were approximated by 0·007 in. wide circumferential saw cuts.

During the fatigue test an oscillatory potential change, synchronous with the strain cycling, was observed, Fig. 6c, insert. The instantaneous crack length was determined from the potential change measured at maximum tensile strain amplitude, less the value obtained prior to crack initiation.

The minimum observable potential change (above the oscillatory value) corresponded to an initiating crack of 0·0002 in. in depth, or approximately 0·15%

[1]) A definite "crack plane" is necessary as the gauge length over which the potential changes are measured must be small to give the required sensitivity. This effectively limits this method to notched specimens which have a well-defined crack plane.

change in the radius of the load bearing (non-cracked) area. The Keithley 150A microvolt/Ammeter used was capable of measuring potentials of 10^{-9} V on the lowest range, i.e. 10^{-7} V full scale. For most tests the 10^{-6} V full scale range was sufficient to determine crack initiation.

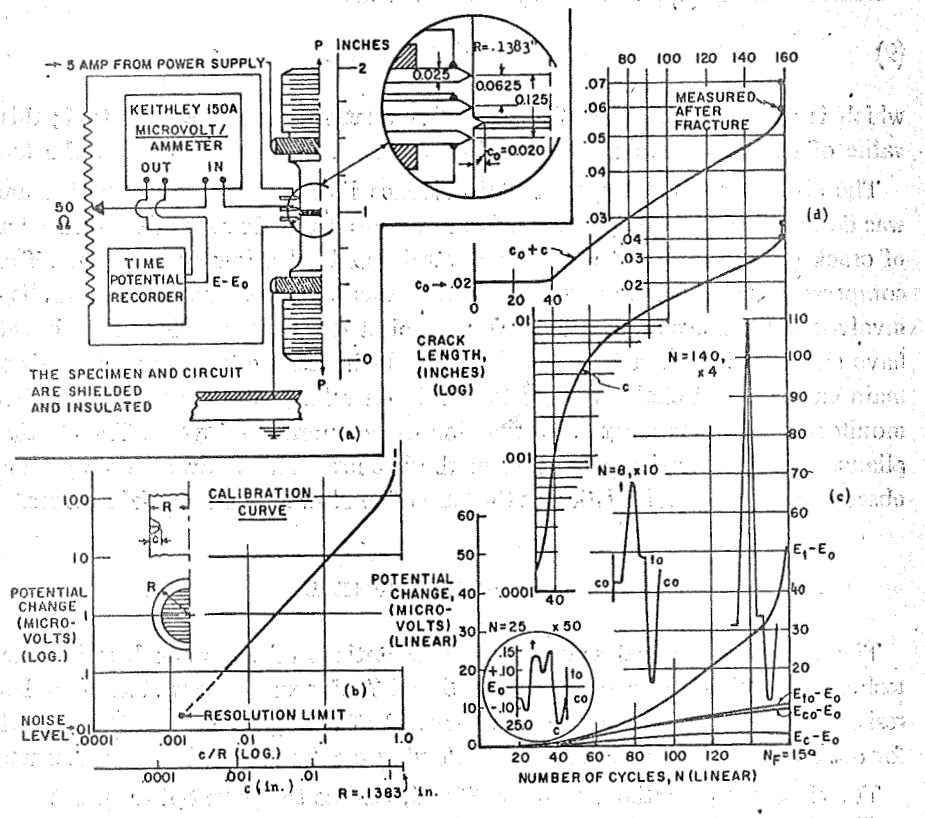

Fig. 6. Electrical potential technique; a) schematic of specimen and knife-edged rings and auxiliary apparatus used in potential measurements, b) empirically determined calibration curve, c) plot of potential change and typical potential recordings observed in a typical fatigue test, d) plot of the log of the crack depth c, measured from the root of the notch and the total crack depth $c_0 + c$, as a function of the number of cycles N, as determined from the calibration curve (b) and the observed change in the potential at maximum tension (c).

The second technique for following crack growth was mechanical and based on the variation of the spring constant with cross sectional area or crack depth.

In these tests, the overall extension is held constant ("strain controlled fatigue"). Following crack initiation, the load required to give the predetermining overall extension drops monotonically until the final fracture occurs. The instantaneous crack length can be determined from the slope of the elastic unloading line in the tensile quadrant of the hysteresis loops, see inserts Fig. 7c. It is customary [10] to relate crack length to compliance C, where the compliance is defined as the elastic extension

per unit load. The required calibration curve, Fig. 7b, was determined simultaneously with the one for the potential measurements. In the calibration, the compliance corresponding to the saw-cut "crack" was determined for elastic loading in the entire cross-section.

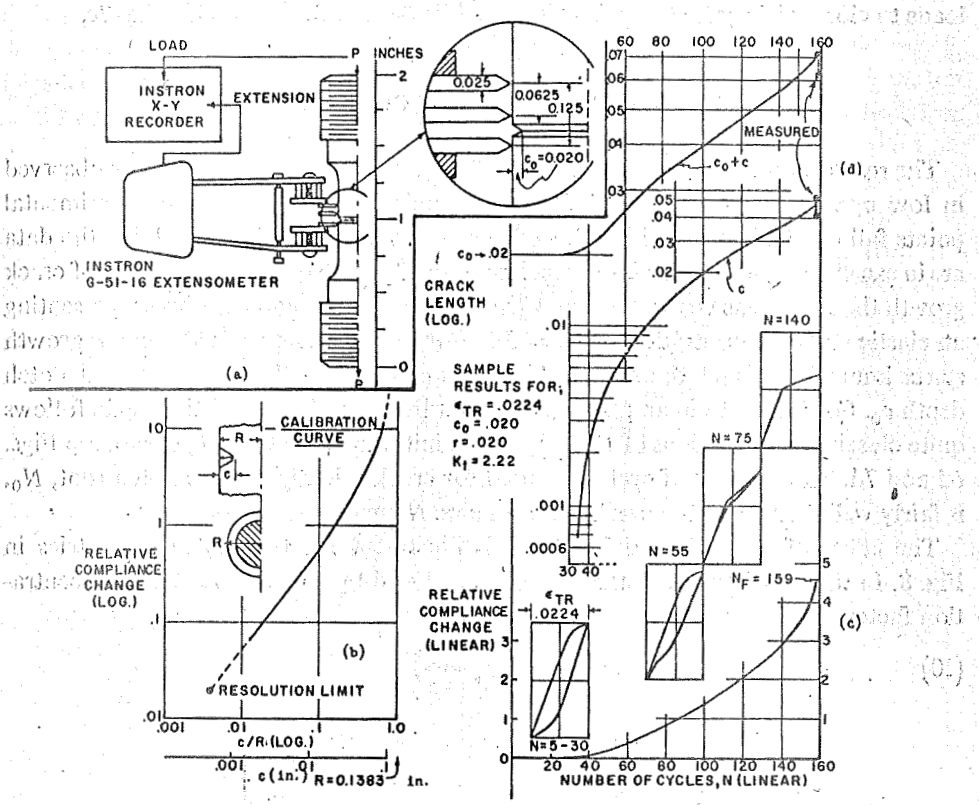

Fig. 7. Compliance technique; a) schematic of specimen and extensometer (attached to the outermost potential measurement rings) used in following compliance changes and controlling the overall extension in the fatigue tests, b) empirically determined calibration curve, c) plot of relative compliance change $(C-C_0)/C_0$ and typical load — extension hysteresis loops observed during the same fatigue test as in Fig. 6, d) plot of log of the crack depths c and $c_0 - c$ versus N, as determined from the calibration curve (b) and the observed compliance changes (c).

The gauge length for the extension measurements was twice that used for the electrical potential measurements. Consequently, the sensitivity of this method is reduced. The minimum resolvable crack depth on initiation using this method was about four times greater than that obtained from the electrical potential method.[2])

In any case, both methods indicated the presence of a crack considerably larger than their respective minimum resolvable sizes within 2–3 cycles of each other and

[2]) Using compliance measurements to follow crack propagation was also limited to notched specimens.

within 1–2 cycles after "crack initiation". From the hysteresis loops shown in the inserts in Fig. 7c it is also apparent that once a crack of sufficient size has developed, i.e. after 75 cycles, it closes under very small compressive loads and represents no stress concentration in the compressive quadrant. Shorter cracks require higher compressive loads to close, giving rise to hysteresis loops like the one for $N = 55$ in Fig. 7c.

3. RESULTS AND DISCUSSION

The results shown in Fig. 5 are typical of the crack propagation behavior observed in low cycle strain controlled fatigue of cylindrical specimens. The experimental points fall on straight lines in a plot of ln c versus number of cycles N, i.e. the data are in excellent agreement with the predictions of Eq. (8). To localize the plane of crack growth the specimens were provided with shallow circumferential grooves representing an elastic stress concentration of $K_t = 3{\cdot}5$. For high strain amplitudes crack growth starts immediately and the straight line extrapolates exactly to the original notch depth c_0. For lower strain amplitudes or longer lives, crack propagation again follows quite closely the predictions of Eq. (8) after an initiation period of N_0 cycles, see Figs. 6d and 7d. The number of cycles required for crack initiation at the notch root, N_0, is fairly well defined by the break in the ln c vs. N curve.

The effect of circumferential notches is illustrated for two notch geometries in Fig. 8. In the very low cycle range the life is reduced by an effective strain concentration factor, K_ε,

$$N^a K_\varepsilon \,.\, \varepsilon_p = \varepsilon_F^* \,. \tag{10}$$

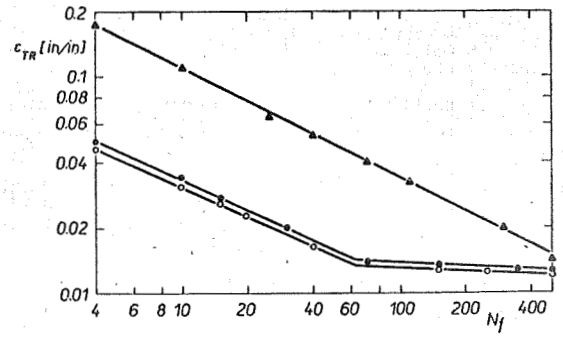

Fig. 8. Total strain range versus number of cycles to failure for three notch geometries ▲ – $K_t = 1$, ● – $K_t = 3{\cdot}5$ ($\varrho = 0{\cdot}003$ in, $c_0 = 0{\cdot}005$ in), ○ – $K_t = 5{\cdot}75$ ($\varrho = 0{\cdot}001$ in, $c_0 = 0{\cdot}007$ in).

Since the loss in life observed in the presence of stress concentrations must be mainly due to a reduction of N_0 and since the curves for smooth and notched specimens are parallel in the extremely low cycle region it was suspected that a Manson-Coffin type

relationship also governs crack initiation. There are two problems in the testing and analysis of notched specimens: the value of the strain concentration factor and of the net section strain amplitude. The strain concentration factor is a function of the strain amplitude and varies, as estimated from Neuber's formula, Eq. (4), between K_t^2 for high plastic strains and K_t for elastic strains. The relationship between K_t and K_ε, determined from the cyclic stress strain curve for Al 7075-T6 is shown in Fig. 9. Because of the notch geometry chosen, no diametral strain measurement across the net section was possible and the strain had to be determined in the longitudinal direction. The reading was consequently a function of the gage length, 0·125 in. for the tests reported here. Hence the strain values quoted are correct only in the relative sense, from one test to another, but the absolute values were not determined. The same uncertainty is present in the apparent strain concentration factor measured from the separation of the two parallel curves in Fig. 8. The observation that the knee in the $\ln \varepsilon_{TR}$ vs. $\ln N$ curves for notched specimens occurs near the nominal strain range for which it would be expected in smooth specimens suggests that the error involved is not very great.

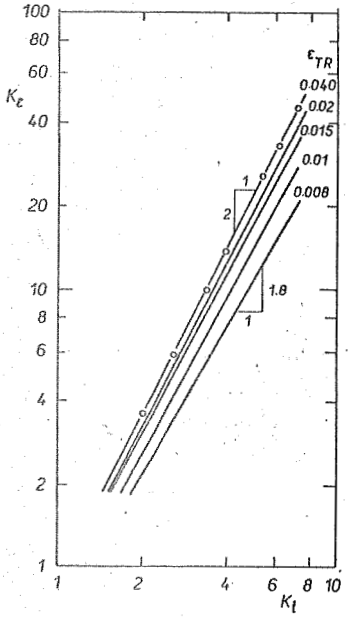

Fig. 9. Strain concentration factor versus theoretical elastic stress concentration factor with the total strain range as a parameter.

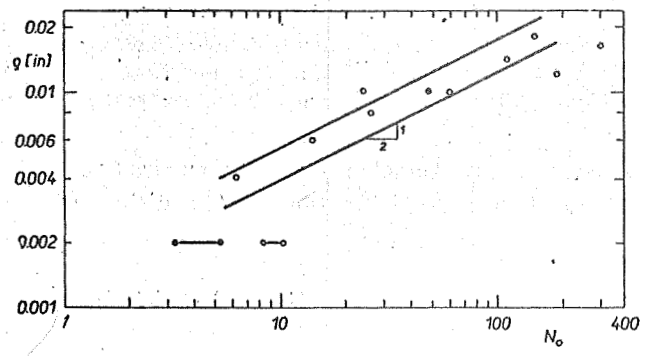

Fig. 10. Root radius versus number of cycles to crack initiation with total strain range constant. Total strain range $\varepsilon_{TR} = 0{\cdot}0150 \pm 0{\cdot}0005$. o — polished, ● — not polished.

The experimental methods used for determining crack growth were sufficiently sensitive to determine the onset of crack propagation at the base of the notch. For the present case crack initiation, N_0, was defined for a crack depth beyond the notch root of approximately 0·0002—0·0005 in. To avoid the ambiguities concerning the net section strain, tests were conducted on a series of test specimens in which only

the notch root radius, ϱ was changed under constant strain range.The results are shown in Fig. 10 where ln N_0 is plotted as a function of ln ϱ. The data follow closely the relationship

$$N_0^{1/2} \cdot \frac{1}{\varrho} = \text{const.} \tag{11}$$

which results from the Eq. (10) with $K_\varepsilon = K_t^2 = 4\, c_0/\varrho$ since ε_p and c_0 were kept constant. This can be considered further evidence that the Manson-Coffin relationship

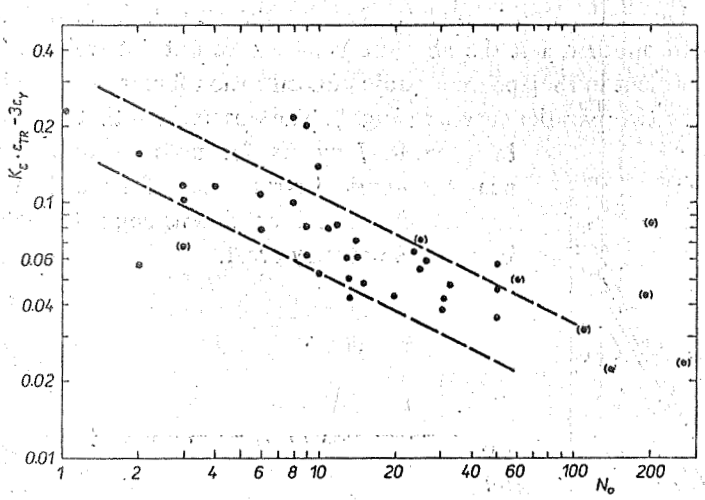

Fig. 11. Effective strain at the notch root versus the number of cycles to crack initiation.

applies not only to crack propagation but also to crack initiation. Since the number of cycles to failure, N_f, is the sum of N_0 and the period of crack propagation N_p, one obtains

$$(N_0 + N_p) = N_f = \frac{\text{const.}}{\varepsilon_p^{1/a}} \tag{12}$$

which is precisely the Manson-Coffin relationship.

A summary of all the data on crack initiation is presented in Fig. 11. This figure is based on the above observations for crack initiation, and the concept that crack initiation may be regarded as failure inside a small region near the base of the notch. The plastic strain range in that region has to be estimated, under consideration of the plastic constraint factor for the notch geometry chosen. For the present estimate a constraint factor of 3 was chosen. To obtain the plastic strain range a value of three times the yield strain was subtracted from the product of net section strain times strain concentration factor. The strain concentration factors were obtained from Neuber's macro-support effect [12] under consideration of a micro support effect

characterized by $\varrho^* = 0{\cdot}0015$ in. The data fall in a scatter band around the relationship

$$N_0^{1/2}(K_\varepsilon \varepsilon_{TR} - 3\varepsilon_Y) = \text{const.} \tag{13}$$

somewhat below the data obtained for the smooth specimens.

Thus it appears that continuum mechanics can provide valuable guidance in the search for fatigue mechanisms, particularly in the low cycle range. While such an analysis cannot be extended to determine the detailed structural mechanisms it gives quantitative information about the breakdown of continuum mechanics, ϱ^*, and of the applicability of linear elasticity, the macro support effect. It is of course directly applicable as a tool for design against low cycle fatigue.

Received 24. 9. 1968.

References

[1] Manson S. S.: Behavior of Materials Under Conditions of Thermal Stress. TN 2933, NACA 1953; Report No. 1170, 1954.
[2] Coffin L. F. Jr.: Trans. ASME *76* (1954), 923.
[3] Sachs G., Gerberich W. W., Weiss V., Latorre J. V.: Proc. Am. Soc. Test. Mat. *60* (1960), 512.
[4] Manson S. S., Hirschberg M. H.: Fatigue Behavior in Strain Cycling in Low and Intermediate Cycle Range. *In book* Fatigue — An Interdisciplinary Approach. Syracuse University Press 1964, 133.
[5] Weiss V.: Analysis of Crack Propagation in Strain-Cycling Fatigue. *In book* Fatigue — An Interdisciplinary Approach. Syracuse University Press 1964, 179.
[6] Weiss V.: Notch Analysis of Fracture. *In* Treatise on Fracture, ed. H. Liebowitz. Academic Press, to be published.
[7] Neuber H.: J. Appl. Mech. XX (1961), 544.
[8] Weiss V.: Am. Soc. Mech. Engr. Paper No. 62-WA-270 (1962).
[9] Liu H. W.: Trans. ASME *83* (1961), 23.
[10] Brown W. F., Srawley J. E.: Fracture Toughness Testing Methods. *In book* Fracture Toughness Testing and its Applications. Am. Soc. Test. Mat. Spec. Tech. Pub. No. 259, 1959.
[11] Neuber H.: Kerbspannungslehre. Springer 1958.
[12] Neuber H.: Theoretical Calculation of the Strength at Stress Concentrations. International Colloquium on the Mechanism of Fatigue, Brno 1968, Czechoslovakia.